The GPIHBP1–LPL complex is responsible for the margination of triglyceride-rich lipoproteins in capillaries

Chris N. Goulbourne[1,*], Peter Gin[1,*], Angelica Tatar[1], Chika Nobumori[1], Andreas Hoenger[2], Haibo Jiang[3], Chris R. M. Grovenor[3], Oludotun Adeyo[1], Jeffrey D. Esko[4], Ira J. Goldberg[5], Karen Reue[1,6], Peter Tontonoz[7,8], André Bensadoun[9], Anne P. Beigneux[1], Stephen G. Young[1,6,‡], and Loren G. Fong[1,‡]

[1]Department of Medicine, David Geffen School of Medicine, University of California Los Angeles, Los Angeles, CA 90095; [2]Department of Molecular, Cellular and Developmental Biology, University of Colorado, Boulder, CO 80309; [3]Department of Materials, University of Oxford, Oxford, United Kingdom; [4]Department of Cellular and Molecular Medicine, University of California San Diego, La Jolla, CA 92093; [5]Department of Medicine, Columbia University, New York, NY 10032; [6]Department of Human Genetics, University of California, Los Angeles, CA 90095; [7]Howard Hughes Medical Institute; [8]Department of Pathology and Laboratory Medicine, University of California, Los Angeles, CA 90095; [9]Division of Nutritional Science, Cornell University, Ithaca, NY 14853

[*]Co-first authors

‡Address correspondence to Loren G. Fong or Stephen G. Young, Department of Medicine, University of California at Los Angeles, 695 Charles E. Young Dr. South, 4506 Gonda Bldg., Los Angeles, CA 90095. Tel: (310) 825-4997; Fax: (310) 267-2722; E-mail: lfong@mednet.ucla.edu, sgyoung@mednet.ucla.edu

Running title

TRL margination depends on an LPL–GPIHBP1 complex

ABSTRACT

Triglyceride-rich lipoproteins (TRLs) undergo lipolysis by lipoprotein lipase (LPL), an enzyme that is transported to the capillary lumen by an endothelial cell protein, GPIHBP1. For LPL-mediated lipolysis to occur, TRLs must bind to the lumen of capillaries. This process is often assumed to involve heparan sulfate proteoglycans (HSPGs), but we suspected that TRL margination might instead require GPIHBP1. Indeed, TRLs marginate along the heart capillaries of wild-type but not *Gpihbp1*$^{-/-}$ mice, as judged by fluorescence microscopy, quantitative assays with infrared-dye–labeled lipoproteins, and EM tomography. Both cell culture and *in vivo* studies showed that TRL margination depends on LPL bound to GPIHBP1. Of note, the expression of LPL by endothelial cells in *Gpihbp1*$^{-/-}$ mice did not restore defective TRL margination, implying that the binding of LPL to HSPGs is ineffective in promoting TRL margination. Our studies show that GPIHBP1-bound LPL is the main determinant of TRL margination in capillaries.

INTRODUCTION

The triglycerides within the core of triglyceride-rich lipoproteins (TRLs; chylomicrons and VLDL) undergo hydrolysis by lipoprotein lipase (LPL) in the capillary lumen, mainly in heart, skeletal muscle, and adipose tissue (1, 2). LPL is synthesized by parenchymal cells, but its site of action is within the capillary lumen. The mechanism by which LPL reaches the capillary lumen was recently solved. LPL in the interstitial spaces is bound by GPIHBP1, a GPI-anchored protein of endothelial cells, and then transported across the cells to the capillary lumen (3, 4). In the setting of GPIHBP1 deficiency, LPL accumulates in the interstitial spaces and cannot reach the capillary lumen, resulting in severe hypertriglyceridemia (chylomicronemia) (3, 5) and reduced delivery of lipid nutrients to parenchymal cells (6). GPIHBP1 is not expressed in endothelial cells of larger blood vessels (*e.g.*, arteries, veins), nor is it expressed in capillaries of the brain (3, 5), an organ that primarily uses glucose for fuel.

For lipolysis to proceed, TRLs in the bloodstream need to stop at the luminal face of capillaries. The partitioning of large TRLs along the capillary endothelium has been aptly called “margination” (7). The molecule(s) on endothelial cells responsible for capturing TRLs in the bloodstream have remained unclear. One possibility, proposed in several reviews (8, 9), is that TRLs bind to the luminal surface of capillaries by interacting with heparan sulfate proteoglycans (HSPGs) lining capillary endothelial cells. This model seems plausible, given that several apolipoproteins on TRLs contain positively-charged heparin–binding domains (*e.g.,* apo-B, apo-AV, apo-E) and are known to bind to negatively-charged HSPGs (10-14). According to this model, lipolysis of TRLs proceeds because of the proximity of HSPG-bound TRLs to LPL in the capillary lumen. In a variation of

this model, HSPG-bound LPL contributes to TRL binding. LPL contains heparin-binding domains that interact with HSPGs and also contains lipid-binding sequences that bind (at least in biochemical assays) TRLs and triglyceride-rich emulsion particles (15, 16). Thus, LPL could bridge capillary HSPGs and TRL particles (17). There is indirect support for this model. When LPL is added to isolated and perfused arteries (where the LPL is presumably attached to HSPGs), there is increased binding of fluorescently labeled TRLs to the arterial wall (14). However, direct investigations of TRL margination *in capillaries* have lagged behind, at least in part because of the absence of experimental approaches to visualize and quantify TRL margination within the microvasculature.

In this study, we sought to define mechanisms for TRL margination in capillaries. We developed techniques for imaging and quantifying TRL margination and examined the possibility that GPIHBP1 might be crucial for this process. We found that GPIHBP1—and more specifically GPIHBP1-bound LPL—is the main determinant of TRL margination in the microvascular circulation.

RESULTS

Binding of triglyceride-rich lipoproteins (TRLs) to small blood vessels in the heart in wild-type mice but not in *Gpihbp1* knockout mice

We hypothesized that TRL margination might require GPIHBP1 and/or GPIHBP1-bound LPL. We began by testing whether TRLs would stop along capillaries in *Gpihbp1*$^{-/-}$ mice. We labeled TRLs (d < 1.006 g/ml lipoproteins from *Gpihbp1*$^{-/-}$ mice) with Alexa555 and injected them intravenously (along with FITC-labeled tomato lectin) into wild-type and *Gpihbp1*$^{-/-}$ mice. After 30 sec, the mice were perfused with PBS to remove unbound lipoproteins, fixed *in situ*, and tissue samples prepared for microscopy. As expected, the tomato lectin bound to endothelial cells (both in capillaries and larger blood vessels). However, the TRLs bound only to heart capillaries in wild-type mice and did not bind to larger blood vessels (Fig. 1A, arrowheads) or to capillaries in the brain (Fig. S1A) (two sites where GPIHBP1 expression is absent) (3, 5). TRL margination was nearly absent in heart capillaries of *Gpihbp1*$^{-/-}$ mice (Fig. 1A). The TRLs in wild-type mice colocalized with GPIHBP1 and LPL (Fig. S1B) and were located along the luminal side of capillary endothelial cells (Fig. 1B). Transmission electron microscopy (EM) demonstrated binding of TRLs to the luminal face of heart capillaries in wild-type mice (Fig. 1C), but there was no TRL binding to heart capillaries of *Gpihbp1*$^{-/-}$ mice (Fig 1C). The identity of injected TRL particles along the surface of capillaries was confirmed by nano-secondary ion mass spectrometry (nanoSIMS) imaging (18). This technique makes it possible to visualize stable isotopes (*e.g.*, ^{13}C) in biological samples with ~50 nm lateral resolution. For these studies, ^{13}C-labeled TRLs from a *Gpihbp1*$^{-/-}$ mouse were injected intravenously into a wild-type and *Gpihbp1*$^{-/-}$ mouse. After 8 min, the

hearts were perfused extensively, fixed, and tissue sections analyzed by nanoSIMS imaging. ^{13}C enrichment in the nanoSIMS images often coincided with lipoproteins at the luminal surface of capillaries in wild-type mice (visualized by low-voltage back-scattered electron microscopy from the same section). No lipoproteins were detected in capillaries of *Gpihbp1*$^{-/-}$ mice (Figs. S1C).

TRLs bind to the open spaces inbetween patches of the glycocalyx

The luminal surface of vascular endothelial cells is covered by a glycocalyx that is rich in glycoproteins and proteoglycans (19, 20). To characterize the binding of TRLs in relation to the endothelial cell glycocalyx, unlabeled TRLs were injected into a wild-type mouse, perfused with PBS to remove unbound lipoproteins, and stained with Alcian blue to visualize the glycocalyx (19). The glycocalyx in large blood vessels (*e.g.*, venules) of the heart appears as a continuous dense "forest" extending ~200 nm above the luminal surface (Fig. 2). In contrast, the glycocalyx in heart capillaries is patchy, with "tufts" of glycocalyx (~75-nm tall) interspersed between open spaces where the plasma membrane is exposed (Fig. 2). A patchy appearance of the glycocalyx has also been observed in rat peritubular capillaries (20). TRLs bound to the gaps between tufts of glycocalyx (Fig. 2; also see tomogram movies S1 and S2).

Identification of "nanovilli" by dual-axis EM tomography and their association with TRLs

We also examined the margination of TRLs by dual-axis electron tomography, making it possible to visualize TRLs in 250-nm-thick sections (21). Consistent with the routine transmission EM studies, multiple TRLs were found on the endothelial cell surface in wild-type mice, but not in *Gpihbp1*$^{-/-}$ mice (Fig. S2). Many TRL particles appeared to be attached to thin plasma membrane

projections located at the luminal surface (Figs. 3A–C and S2). The projections on the luminal surface were 6.6 ± 0.3 nm (n = 21) in diameter and ranged in height from 100 to 200 nm. The same membrane projections were also found within caveolar-like invaginations of endothelial cells (Fig. 3D–E), in transcytotic vesicles or channels (Fig. 3D–F), and on the plasma membrane at the basolateral face of cells (Fig. 3E). These structures were also found in heart capillary endothelial cells of *Gpihbp1*$^{-/-}$ mice, but not in adjacent myocytes (Fig. S2). Electron microscopy did not reveal any cytoplasm or structural elements (*e.g.*, actin filaments) within the membrane projections, but they had the hallmark "railroad-track morphology" of lipid bilayers (22) (Fig. 3F). These structures, which we have called "nanovilli," had not been noted previously, almost certainly because clear visualization of these structures requires EM tomography (they are infrequent and subtle by routine transmission EM). To determine whether nanovilli might contain GPIHBP1, we performed immunogold labeling with a GPIHBP1-specific rat monoclonal antibody. In preliminary studies, detection of GPIHBP1 was limited when primary or secondary antibodies were conjugated to colloidal gold. We therefore used unlabeled anti-GPIHBP1 antibodies along with anti-rat Fab′ fragments conjugated to 1.4-nm gold beads. Using 1.4-nm beads requires that tissue sections be treated with silver enhancement solutions to produce particles large enough to detect by EM. Transmission EM demonstrated many silver-enhanced gold particles on capillary endothelial cells in wild-type mice, but none in *Gpihbp1*$^{-/-}$ mice (Fig. S2). Most of the gold particles were located on the luminal surface, especially within caveolae-like invaginations, but they were also detected within intracellular vesicles and on the basolateral surface. To determine if gold particles were also on nanovilli, EM tomography was performed. Unfortunately, the silver enhancement procedure interferes with

the osmium and uranyl acetate staining of membranes, including nanovilli. However, linear “strings” of gold particles projecting into the capillary lumen (and within endothelial cell vesicles) were often found by EM (Fig. 3G–I).

Quantitative measurement of TRL margination *in vivo*

To quantify TRL margination, mice were injected with lipoproteins that had been labeled with infrared (IR) dyes. In these studies, wild-type and *Gpihbp1*$^{-/-}$ mice were pretreated with tetrahydrolipstatin (THL) to prevent lipolysis. After 30 sec, the mice were perfused extensively, first with PBS and then with fixative. Next, frozen sections of mouse tissues were cut, and the level of each IR-dye in tissue sections was quantified with an infrared scanner. In initial studies, we compared the binding of IR800-dye–labeled TRLs and IR680-dye–labeled cholesterol ester–rich mouse β-VLDL. IR800-dye–labeled TRLs bound avidly to the heart, liver, and brown adipose tissue (BAT) of wild-type mice, while TRL binding in the brain was nearly undetectable (Fig. 4A–B). In *Gpihbp1*$^{-/-}$ mice, the binding of TRLs to the liver was similar to that observed in wild-type mice, but the binding of TRLs to heart and BAT was lower. IR680-dye–labeled β-VLDL bound avidly to the liver, but binding to heart and adipose tissue was low in both wild-type and *Gpihbp1*$^{-/-}$ mice (Fig. 4C–D).

The binding of IR-dye–TRLs to the heart was heparin-sensitive and was lower in *Gpihbp1*$^{-/-}$ mice than in wild-type mice when normalized to tissue area or to endothelial cell content (Fig. S3A–B). Like TRLs isolated from the plasma of *Gpihbp1*$^{-/-}$ mice, IR-dye–labeled human VLDL bound avidly to wild-type mouse hearts, but binding to *Gpihbp1*$^{-/-}$ hearts was low (Fig. S3C). In contrast, IR-dye–labeled HDL bound poorly to wild-type mouse hearts but bound avidly to adrenal glands in both wild-type and *Gpihbp1*$^{-/-}$ mice (Fig. S3D). The binding of TRLs to

the heart was also examined with other IR dyes (*e.g.,* IR680, maleimide-IR800) but the results were the same: the binding of TRLs to the heart depended on GPIHBP1 and could be blocked with heparin.

The reduced binding of TRLs in *Gpihbp1*$^{-/-}$ mouse hearts is not due to high plasma triglyceride levels

We considered the possibility that reduced binding of labeled TRLs to heart capillaries in *Gpihbp1*$^{-/-}$ mice was somehow the consequence of higher levels of TRLs in the plasma of those mice. However, two lines of evidence showed that this was not the case. The first involved studies with isolated, perfused hearts. Hearts from *Gpihbp1*$^{-/-}$ mice were perfused extensively with buffer (to remove all lipoproteins) and then with buffer containing Alexa555-labeled–TRLs, Alexa647-labeled–rat IgG, and FITC-labeled–lectin. After 5 min at 4° C, hearts were perfused extensively with buffer to remove unbound materials. The tomato lectin bound to endothelial cells in wild-type and *Gpihbp1*$^{-/-}$ mice; however, TRLs bound only to the capillaries of wild-type mice and not to capillaries of *Gpihbp1*$^{-/-}$ mice (Fig. S4A). Occasional spots of "TRL binding" were detected in *Gpihbp1*$^{-/-}$ hearts, but those were invariably explained by inadequate perfusion with buffer (the same spots were positive for Alexa647-labeled–rat IgG). The second line of evidence came from *in vivo* TRL margination studies in *Gpihbp1*$^{-/-}$*Angptl4*$^{-/-}$ mice (23), which have much lower plasma triglyceride levels than *Gpihbp1*$^{-/-}$ mice (132 mg/dl in *Gpihbp1*$^{-/-}$*Angptl4*$^{-/-}$ mice *vs*. 1742 mg/dl in *Gpihbp1*$^{-/-}$ mice; n = 3/group). The lower triglyceride levels are consistent with the marked increase in chylomicron metabolism by macrophages in the lymphatics of *Angptl4*$^{-/-}$ mice (24). The margination of IR-dye–labeled TRLs was absent in the heart capillaries of both *Gpihbp1*$^{-/-}$*Angptl4*$^{-/-}$ and *Gpihbp1*$^{-/-}$ mice (Fig. S4B). As

expected, LPL was absent from the capillary lumen in both *Gpihbp1*$^{-/-}$ and *Gpihbp1*$^{-/-}$*Angptl4*$^{-/-}$ mice (Fig. S4C).

The binding of TRLs and lipid emulsions (Intralipid) to cultured cells depends on GPIHBP1 and on the lipid-binding domain of LPL

The failure of TRLs to marginate within heart capillaries of *Gpihbp1*$^{-/-}$ mice indicates the importance of GPIHBP1 in this process. However, given GPIHBP1's role in binding LPL and shuttling it to the capillary lumen, it seemed possible that TRL binding might also require GPIHBP1-bound LPL. Indeed, previous studies have suggested that GPIHBP1-expressing CHO cells have little ability to bind TRLs in the absence of LPL (25). This would also be consistent with the inhibition of TRL margination in wild-type mice by heparin (Fig. S3A). Here, we pursued this possibility by examining TRL binding to GPIHBP1-expressing CHL-11 cells, which produce only negligible amounts of LPL (25). Again, we found no TRL binding to those cells unless they were first pre-incubated with LPL (Fig. 5A). To further explore the role of GPIHBP1-bound LPL in TRL binding, we tested whether the LPL-specific monoclonal antibody 5D2 would be capable of blocking TRL binding. [Antibody 5D2 binds to residues 380–410 of human LPL and blocks the delivery of long-chain triglyceride substrates to LPL's catalytic domain (16, 26, 27).] Interestingly, antibody 5D2 nearly abolished binding of TRLs to GPIHBP1–LPL complexes on the surface of CHL-11 cells, whereas a mouse monoclonal antibody against the V5-tag had no effect (Fig. 5A). To further assess the role of GPIHBP1-bound LPL in capturing TRL particles, we mutated a cluster of tryptophans in LPL (W390A/W393A/W394A) that are known to be important for triglyceride hydrolysis by LPL's catalytic domain (and for the epitope of antibody 5D2) (16); and see Fig. S5C). The

mutant LPL bound avidly to GPIHBP1, but the mutant LPL–GPIHBP1 complex could not bind TRLs (Fig. S5A). Mutating single tryptophan residues yielded an intermediate phenotype (Fig. S5A). These studies implied that GPIHBP1-bound LPL binds TRLs and that the same LPL sequences that are important for delivering triglyceride substrates to LPL's catalytic domain are responsible for binding TRL particles on the surface of cells.

We also examined the ability of GPIHBP1–LPL complexes on cells to bind triglyceride emulsion particles (Intralipid). Fluorescently-labeled (DiI) Intralipid did not bind to nontransfected or GPIHBP1-transfected CHL-11 cells but did bind to GPIHBP1-expressing cells that had been pre-incubated with LPL (Fig. 5B). The binding of Intralipid to cells could be blocked with antibody 5D2 (Fig. 5B) or by blocking LPL binding to GPIHBP1 with heparin (Fig. S5B).

TRLs bind to a GPIHBP1–LPL complex *in vivo*

The cell culture studies indicated that GPIHBP1 has little ability to bind TRLs in the absence of LPL. To assess the *in vivo* relevance of these findings, we pursued two experimental approaches. The first was to investigate the ability of TRLs to stop in lung capillaries. Unlike heart and BAT, which express high levels of both LPL and GPIHBP1, the lung expresses high levels of GPIHBP1 but almost no LPL (28). IR-dye–labeled TRLs did not marginate along lung capillaries in wild-type mice (Fig. S6). However, the lungs are able to capture LPL from the circulation (28, 29), and after an intravenous injection of purified bovine LPL, LPL levels increased in the lung (Fig. S7A) and bound TRLs avidly (Fig. 6A). In contrast, when bovine LPL was injected into *Gpihbp1*$^{-/-}$ mice, there was only a small increase in TRL binding in the lungs (Fig. 6A).

The second approach to investigate the importance of GPIHBP1-bound LPL for TRL binding was to asess TRL margination in the hearts of "L0-MCK" mice [homozygous *Lpl* knockout mice that carry a human LPL transgene driven by the muscle creatine kinase (MCK) promoter]. These mice express small amounts of human LPL in the heart (30) and is transported to the capillary lumen by GPIHBP1. The binding of IR-dye–labeled TRLs to hearts of L0-MCK mice was greater than in *Gpihbp1*$^{-/-}$ mice but less than in wild-type mice (Fig. 6B). An intravenous injection of antibody 5D2 (which binds to human LPL) lowered TRL binding in hearts of L0-MCK mice to levels observed in *Gpihbp1*$^{-/-}$ mice. Antibody 5D2 does not bind to mouse LPL and did not inhibit TRL binding to hearts of wild-type mice (Fig. S7B).

Measurement of HSPG's role in TRL margination *in vivo*

Our studies showed that GPIHBP1-bound LPL has a major role in TRL margination, but based on the residual binding of TRLs in *Gpihbp1*$^{-/-}$ mouse tissues it seemed possible that endothelial cell HSPGs might play a role. LPL contains positively charged heparin-binding domains that are known to bind to negatively charged sulfates on HSPGs. We tested the role of HSPG-bound LPL in TRL margination in two ways. First, we quantified the margination of TRLs in mice that lack NDST1 (*N*-deacetylase/*N*-sulfotransferase1) in endothelial cells (*Ndst1*$^{fl/fl}$*Tek-Cre*) (31). NDST1 adds sulfates to HSPGs, and when this enzyme is absent, HSPG sulfation is reduced by ~50% (32). When IR-dye–labeled TRLs were injected into *Ndst1*$^{fl/fl}$*Tek-Cre* mice, the binding of the TRLs to the heart was not reduced and actually appeared to be increased. In the same hearts, the binding of IR-dye–labeled acetyl-LDL (a chemically modified LDL that binds to endothelial cells) was unaffected by a deficiency of NDST1 (Fig. S7C).

In a second approach, we measured TRL margination in mice that express human LPL in endothelial cells [EC-hLPLH transgenic mice; (33)]. LPL is normally produced by myocytes in the heart and requires GPIHBP1 to move it across endothelial cells to the capillary lumen. However, in EC-hLPLH mice, catalytically active LPL would likely be secreted directly into the circulation and have the opportunity to bind to endothelial cell HSPGs. If some of this LPL attaches to HSPGs, and if the HSPG–LPL complex is involved in TRL margination, then TRL margination should be higher in *Gpihbp1*$^{-/-}$EC-hLpLH mice than in *Gpihbp1*$^{-/-}$ mice. However, TRL margination in the heart was unaffected; the binding of TRLs to heart capillaries of *Gpihbp1*$^{-/-}$EC-hLpLH mice was no greater than in *Gpihbp1*$^{-/-}$ mice (Fig. 7). To verify that some of the EC-derived hLPL was *intravascular*, plasma hLPL levels were measured after an injection of heparin. To circumvent potential problems relating to the release of *mouse* LPL by heparin, we measured hLPL levels in mice that lacked mouse LPL (*i.e.*, *Gpihbp1*$^{-/-}$EC-hLpLH*Lpl*$^{-/-}$ and EC-hLpLH*Lpl*$^{-/-}$ mice). Plasma samples were obtained 5 minutes after heparin because LPL appearance at that time point reflects release from intravascular sites (34). As expected, preheparin hLPL levels were low in both *Gpihbp1*$^{-/-}$EC-hLpLH*Lpl*$^{-/-}$ and EC-hLpLH*Lpl*$^{-/-}$ mice [0.13 ± 0.004 μg/ml (n = 4) and 0.13 ± 0.05 μg/ml (n = 5), respectively]. The postheparin LPL levels were markedly increased in both groups of mice: 19.88 ± 2.18 μg/ml (n = 4) in EC-hLpLH*Lpl*$^{-/-}$ mice and 3.61 ± 0.80 μg/ml (n = 5) in *Gpihbp1*$^{-/-}$EC-hLpLH*Lpl*$^{-/-}$ mice.

DISCUSSION

In the current studies, we show that GPIHBP1 is crucial for TRL margination in the heart. Two observations support this conclusion. First, in wild-type mice, the ability of endothelial cells to bind fluorescently labeled TRLs correlates with GPIHBP1 expression. TRL binding was robust in capillaries, where GPIHBP1 is expressed at high levels, but virtually undetectable in larger blood vessels, where GPIHBP1 is absent. Second, TRL margination is negligible in capillaries of *Gpihbp1*$^{-/-}$ mice, as judged by immunofluorescence microscopy, transmission EM, and laser-scanning quantification of IRdye-labeled TRL binding in tissues. The failure of TRLs to bind to capillaries of *Gpihbp1*$^{-/-}$ mice was not due to high plasma triglyceride levels because we observed the same results in experiments with isolated, perfused hearts. Also, TRLs failed to marginate in heart capillaries of *Gpihbp1*$^{-/-}$*Angptl4*$^{-/-}$ mice and *Gpihbp1*$^{-/-}$EC-hLpLH mice, where plasma triglyceride levels are far lower. Studies in cultured cells and live mice demonstrated the importance of GPIHBP1-bound LPL for TRL margination. In cultured cells, neither TRLs nor Intralipid particles bound to GPIHBP1-expressing cells unless the cells were first pre-incubated with LPL. Also, the binding of TRLs and Intralipid to GPIHBP1–LPL complexes on the surface of cells could be blocked with the LPL-specific monoclonal antibody 5D2—or by releasing LPL from GPIHBP1 with heparin. In live mice, heparin lowered TRL margination to the low levels observed in *Gpihbp1*$^{-/-}$ mice. Also, TRLs did not bind to GPIHBP1-rich capillaries of the lung, a tissue that does not express LPL, unless the mice were first injected with LPL. Finally, the margination of TRLs in hearts of L0-MCK mice could be blocked with monoclonal antibody 5D2.

It has often been proposed that TRL margination depends on interactions

between positively charged regions in TRL apolipoproteins with negatively charged HSPGs (8, 9). This model seems plausible, given that several apolipoproteins on the surface of TRLs (*e.g.,* apo-B, apo-AV, apo-E) have heparin–binding domains and bind to negatively-charged HSPGs (10-13). In a variation on this model, HSPG-bound LPL plays a role in TRL binding. However, we were unable to document a major role for HSPGs in TRL margination in the heart. TRL margination in heart capillaries of endothelial cell-specific *Ndst1* knockout mice was not reduced. Consistent with this finding, inactivation of *Ndst1* in endothelial cells did not affect the amount of LPL that enters the plasma after an injection of heparin (34). Moreover, an endothelial cell-specific LPL transgene was unable to increase the low TRL margination in *Gpihbp1* knockout mice. In these mice, substantial amounts of human LPL could be released into the bloodstream with an injection of heparin (3.6 μg hLPL/ml plasma). Presumably, this LPL was bound to HSPGs on the luminal surface of blood vessels. If an LPL–HSPG complex was highly effective in mediating TRL binding, one might have expected higher TRL binding in *Gpihbp1*$^{-/-}$EC-hLpLH mice than in *Gpihbp1*$^{-/-}$ mice. However, this was not the case, underscoring the importance of endothelial cell GPIHBP1 in LPL binding and TRL margination in the heart.

A recent study by Bartelt *et al*. (35) showed that an injection of heparin into wild-type mice blocked the margination of triglyceride-rich particles along capillaries of brown adipose tissue (BAT). Their studies did not address whether the inhibition of margination was due to heparin's ability to block interactions between HSPGs and the particles or to heparin's ability to release LPL from the surface of capillaries. The current studies show that the inhibition is mainly due to the heparin-mediated release of LPL from GPIHBP1.

LPL is enzymatically active only as a head-to-tail homodimer (36) and it appears likely that a tryptophan-rich motif within the carboxyl terminus of one monomer delivers triglyceride substrates to the amino-terminal catalytic domain of the partner monomer. In support of this idea, transfection of two catalytically inactive LPLs—one with a mutation in the carboxyl-terminal lipid-binding motif and the other with a mutation in the amino-terminal catalytic domain—yields catalytically active LPL (37). Mutating LPL's carboxyl-terminal tryptophan-rich cluster or incubating LPL with antibody 5D2 (which binds to this region of the molecule) blocks the hydrolysis of triolein (16, 26). Our current studies showed that the same interventions block TRL binding to GPIHBP1–LPL complexes, both on cultured cells and in capillaries of live mice. Thus, we identified an unexpected simplicity in LPL action: the same carboxyl-terminal LPL sequences required for catalysis are critical for the margination of TRL particles in capillaries.

An intriguing finding in the current studies was the discovery, by dual-axis EM tomography, of ~6-nm-thick planes of lipid bilayer, which we have called nanovilli, that extend from the surface of endothelial cells into the capillary lumen. The same membrane bilayer structures are found in transcytotic vesicles and on the basolateral face of endothelial cells. The membrane bilayer structures appear as "sticks" on single EM micrographs; however, when tomographic images are assembled into a movie, the overall structure is evident—they are not sticks but lipid bilayer "planes" (~6 nm thick, 30–40 nm long, and 100–200 nm tall). As far as we are aware, these membrane bilayers have not been described previously, likely because most ultrastructural studies of heart capillary endothelial cells have been conducted with routine transmission EM. While these structures can be identified by transmission EM, they are not as clear and they are easier to overlook and/or dismiss. It seems likely that these structures contain GPIHBP1

and LPL because they were found in close association with TRLs and because we often detected, by immunogold EM, linear “strings” of gold particles extending into the capillary lumen and in intracellular vesicles (the same sites where nanovilli are observed by dual-axis tomography). In the immunogold EM studies, silver enhancement of the 1.4-nm gold beads interfered with osmium tetroxide/uranyl acetate staining of membranes, making it difficult to visualize lipid bilayers underlying the strings of gold particles. Earlier EM studies described endothelial cell “projections” that bulged into the capillary lumen, especially near endothelial cell junctions (38, 39). However, those projections contain abundant cytoplasm and are quite distinct from the membrane bilayer structures that we have described.

In summary, we have used biochemical, imaging, and electron microscopy approaches to study the mechanisms of TRL margination in cultured cells and in new mouse models. We have also developed new quantitative methods to assess TRL margination in live animals. Our studies show that TRL margination depends on GPIHBP1-bound LPL and specifically on sequences within the carboxyl terminus of LPL. HSPGs do not appear to have a large quantitative role in margination. The studies also identified a new endothelial cell structure, which we have called nanovilli. Given the association of nanovilli with TRLs, we speculate that these structures play a role capturing TRL particles along capillaries.

EXPERIMENTAL PROCEDURES

Measurement of lipoprotein binding in tissues. Mice were injected intravenously with 50 µl of 5 mM tetrahydrolipstatin (THL). After 2 min, the mice were injected intravenously with 50–100 µg IR-dye–labeled lipoproteins (see Supplemental information). After 30 sec, the mice were perfused with 15 ml ice-cold PBS to remove unbound lipoproteins, followed immediately by 10 ml ice-cold 3% PFA in PBS. Tissue samples were frozen in O.C.T., and 10-µm-thick sections were placed onto glass slides and scanned with an Odyssey infrared imager. The IR signal for each channel was measured and normalized to tissue area. Tissue area was determined with ImageJ software. The results are reported as the mean ± s.d. Each experiment was done at least three times and only representative experiments are shown, except where indicated.

Lipoprotein binding in isolated perfused hearts. Anesthetized mice were injected intravenously with 50 µl of 5 mM THL. After 2 min, the mice were perfused with 10 ml of Tyrode's solution [136 mM NaCl, 5.4 mM KCl, 0.33 mM NaH_2PO_4, 1 mM $MgCl_2$, 10 mM Hepes (pH 7.4), 10 mM glucose] through the inferior vena cava. The hearts were removed and the aorta cannulated with a blunt-end 20-gauge needle and secured with a suture. The hearts were flushed with Tyrode's solution, submerged in 30 ml Tyrode's solution, and perfused with a 1-ml solution containing 100 µg/ml Alexa555-labeled TRLs, 50 µg/ml FITC-labeled lectin, and 25 µg/ml Alexa647-labeled rat IgG. After 5 min, the hearts were perfused with 10 ml Tyrode's solution followed by 5 ml of 3% PFA in PBS. The hearts were frozen in O.C.T. and processed for fluorescence microscopy (see Supplemental information).

Detection of TRL binding in the heart by transmission electron microscopy and dual-axis electron tomography. Mice were injected with THL and TRLs (50–100 µg) as described for the IR-dye–labeled lipoproteins. After 30 sec, tissues were perfusion-fixed *in situ* with 2.5% glutaraldehyde containing 2 mM $MgCl_2$ in 100 mM cacodylate buffer (pH 7.4) and incubated in the fixation solution at 4° C overnight. The following day, the tissues were incubated in an equal volume of 1% osmium tetroxide and 0.1 M imidazole (pH 7.5). The samples were then washed three times in distilled water (10 min each). Samples were then treated with 1% osmium tetroxide in 100 mM cacodylate buffer for 1 h, washed in distilled water four times (10 min each), and then treated with 1–2% aqueous uranyl acetate overnight at 4º C in the dark. The samples were sequentially dehydrated with increasing concentrations of acetone (20, 30, 50, 70, 90, and 100%) for 30 min each, followed by three additional treatments with 100% acetone for 20 min each. Samples were then infiltrated with increasing concentrations of epon or Spurr's resin (25% for 1 h, 50% for 1 h, 75% for 1 h, 100% for 1 h, 100% overnight at room temperature), and then incubated overnight at 70° C in a resin mold. 50–90-nm-thick sections were cut with a Leica ultramicrotome.

For routine transmission electron microscopy (EM), samples were examined with a 100CX JEOL electron microscope. For EM tomography, 250-nm thick sections were collected on formvar-coated copper slot grids. Following staining, 15-nm colloidal gold particles were applied to both surfaces of the grid to serve as fiducial markers for subsequent image analysis. Dual-axis tilt series (–65º to +65º at 1º intervals) were obtained with a computerized tilt stage with an FEI Tecnai TF30 and Tecnai TF20 electron microscopes operating at 300 kV and

200 kV, respectively. Tomographic reconstruction and modeling was performed with the IMOD software package (21).

Detection of TRL margination by high-resolution (nano) secondary ion mass spectrometry (nanoSIMS). Endogenously labeled ^{13}C-TRLs were harvested from *Gpihbp1*$^{-/-}$ mice after delivering a mixture of ^{13}C-labeled Algal fatty acids (Sigma 487937) by gavage. TRLs were isolated by ultracentrifugation and 50 µg were injected into mice. After 8 min, the mice were perfused with PBS to remove unbound lipoproteins, followed by glutaraldehyde fixative. Tissue samples were processed as described for transmission EM except that 500-nm thick sections were cut and placed onto platinum-coated coverslips.

A CAMECA NanoSIMS 50 was used to acquire chemical and isotopic images**.** The instrument uses a 16 keV primary Cs^+ ion beam to bombard the sample surface and five selected secondary ions were detected to form composition maps with ~50-nm spatial resolution. The ratio between the counts of ^{12}C- and ^{13}C-secondary ions was used to show the distribution of ^{13}C-labeled lipids; the ^{16}O-, ^{12}C^{14}N-, and ^{31}P-signals were also collected to show the morphology of the samples. The smallest primary aperture (D1=4) was used to achieve high spatial resolution images of capillaries (10 × 10 µm, 256 × 256 pixels). The ^{13}C/^{12}C-hue saturation images (HSI) were processed by the OpenMIMS plug-in (MIMS, Harvard University; www.nrims.harvard.edu) in ImageJ software, and processed by a median filter with three-pixel radius. All sections analyzed by NanoSIMS were also studied by low voltage Back Scattered Electron (BSE) imaging at 2kV in a Zeiss NVision FIB to allow direct correlation of the chemical information with the sample structure.

Detection of GPIHBP1 by transmission electron microscopy. Isolated mouse hearts were perfused with 1.0 ml Tyrode's buffer containing 50 µg/ml of a rat anti-GPIHBP1 antibody (clone 11A12). After incubating for 5 min at RT, unbound antibody was removed by perfusing with 5 ml of Tyrode's buffer. Bound antibody was detected by incubation with 36 µg/ml Alexa488-labeled goat anti–rat Fab′ fragments coupled to 1.4-nm gold particles (Nanoprobes, Yaphank, NY). The heart was perfusion-fixed with glutaraldehyde and incubated in the fixative at 4° C. Small pieces of tissue (~1-mm cubes) were treated with an HQ Silver Enhancement Kit (Nanoprobes) according to the manufacturer's instructions and then processed for EM as described earlier.

Binding of TRLs to *Gpihbp1*-transfected cells. CHL-11 cells were plated on coverslips in 24-well plates and transfected with either 0.8 µg of an S-protein–tagged *Gpihbp1* expression vector or empty vector using Lipofectamine 2000 (Invitrogen). After 24 h, the cells were washed with binding buffer (PBS containing 1.0 mM $CaCl_2$, 1.0 mM $MgCl_2$, and 0.5% BSA) and incubated at 4° C for 1 h with 400 µl of concentrated conditioned medium from cells expressing V5-tagged human LPL. LPL mutants were generated by site-directed mutagenesis with the QuikChange Lightning kit (Agilent). All constructs were validated by DNA sequencing. Some cells were also incubated with mouse monoclonal antibody 5D2 (10 µg/ml) or a mouse monoclonal antibody against the V5 tag (10 µg/ml, Invitrogen) at 4° C for 1 h. Cells were then washed three times with binding buffer and incubated with 0.5 ml DiI-labeled TRLs (1 mg/ml) in binding buffer at 4° C for 2 h (25). The cells were washed to remove unbound TRLs, fixed with 3% PFA, blocked, and incubated with a rabbit polyclonal antibody against the S-protein tag (0.4 µg/ml) and a mouse monoclonal antibody against V5 (4 µg/ml). After

washing, the cells were incubated with Alexa488-labeled donkey anti–rabbit IgG (1:500) and an Alexa647-labeled donkey anti–mouse IgG (1:500). After the removal of unbound secondary antibodies, the cells were stained with DAPI to visualize nuclei. Images were captured on an Axiovert 200M microscope (equipped with an LSM 700 confocal scanning module) and processed with the Zen 2010 software. The exposure conditions for each experimental condition were fixed and identical.

ACKNOWLEDGEMENTS

We thank Dr. John Brunzell (University of Washington) for monoclonal antibodies 5D2 and 5F9, Ms. Jinny Wong (Gladstone Institutes) for assisting with some of the EM studies, Ms. Cynthia Page (University of Colorado) for collecting EM tomograms, and Mr. Richard Barnes for measuring triglyceride levels in the *Gpihbp1*$^{-/-}$*Angptl4*$^{-/-}$ mice. This work was supported by grants from the NIH (HL089781, HL090553, HL087228, HL094732, HL45095, and GM33063), the Leducq Transatlantic Network TNT (12CVD04), the American Heart Association, Western States Affiliate (11POST6600001 and 13POST15700001), and the China Scholarship Council. The authors have no financial interests related to this study to declare.

REFERENCES

1. Brunzell, J.D. and Deeb, S.S. (2001) Familial lipoprotein lipase deficiency, apo C-II deficiency, and hepatic lipase deficiency. In Scriver, C.R., Beaudet, A.L., Sly, W.S., Valle, D., Childs, B., Kinzler, K.W. and Vogelstein, B. (eds.), *The Metabolic and Molecular Bases of Inherited Disease.* 8th ed. McGraw-Hill, New York, Vol. 2, p. 2789–2816.

2. Havel, R.J. and Kane, J.P. (2001) Introduction: Structure and metabolism of plasma lipoproteins. In Scriver, C.R., Beaudet, A.L., Sly, W.S., Valle, D., Childs, B., Kinzler, K.W. and Vogelstein, B. (eds.), *The Metabolic and Molecular Bases of Inherited Disease.* 8th ed. McGraw-Hill, New York, Vol. 2, p. 2705–2716.

3. Davies, B.S.J., Beigneux, A.P., Barnes II, R.H., Tu, Y., Gin, P., Weinstein, M.M., Nobumori, C., Nyrén, R., Goldberg, I.J., Olivecrona, G. *et al.* (2010) GPIHBP1 is responsible for the entry of lipoprotein lipase into capillaries. *Cell Metab.,* **12,** 42–52.

4. Davies, B.S., Goulbourne, C.N., Barnes, R.H., 2nd, Gin, P., Vaughan, S., Vaux, D.J., Bensadoun, A., Beigneux, A.P., Fong, L.G. and Young, S.G. (2012) Assessing mechanisms of GPIHBP1 and lipoprotein lipase movement across endothelial cells. *J. Lipid Res.,* **53,** 2690–2697.

5. Beigneux, A.P., Davies, B., Gin, P., Weinstein, M.M., Farber, E., Qiao, X., Peale, P., Bunting, S., Walzem, R.L., Wong, J.S. *et al.* (2007) Glycosylphosphatidylinositol-anchored high density lipoprotein–binding protein 1 plays a critical role in the lipolytic processing of chylomicrons. *Cell Metab.,* **5,** 279–291.

6. Weinstein, M.M., Goulbourne, C.N., Davies, B.S., Tu, Y., Barnes, R.H., 2nd, Watkins, S.M., Davis, R., Reue, K., Tontonoz, P., Beigneux, A.P. *et al.* (2011) Reciprocal metabolic perturbations in the adipose tissue and liver of GPIHBP1-deficient mice. *Arterioscler. Thromb. Vasc. Biol.,* **32,** 230–235 [PMC3281771].

7. Stalenhoef, A.F.H., Malloy, M.J., Kane, J.P. and Havel, R.J. (1986) Metabolism of apolipoproteins B-48 and B-100 of triglyceride-rich lipoproteins in patients with familial dysbetalipoproteinemia. *J. Clin. Invest.,* **78,** 722–728.

8. Goldberg, I.J. (1996) Lipoprotein lipase and lipolysis: Central roles in lipoprotein metabolism and atherogenesis. *J. Lipid Res.,* **37,** 693–707.

9. Cryer, A. (1989) The role of the endothelium in myocardial lipoprotein dynamics. *Mol. Cell Biochem.,* **88,** 7–15.

10. Cardin, A.D., Barnhart, R.L., Witt, K.R. and Jackson, R.L. (1984) Reactivity of heparin with the human plasma heparin-binding proteins thrombin,

antithrombin III, and apolipoproteins E and B-100. *Thromb. Res.,* **34,** 541-550.

11. Brown, M.S. and Goldstein, J.L. (1986) A receptor-mediated pathway for cholesterol homeostasis. *Science,* **232,** 34–47.
12. Cardin, A.D., Hirose, N., Blankenship, D.T., Jackson, R.L. and Harmony, J.A.K. (1986) Binding of a high reactive heparin to human apolipoprotein E: Identification of two heparin-binding domains. *Biochem. Biophys. Res. Commun.,* **134,** 783–789.
13. Lookene, A., Beckstead, J.A., Nilsson, S., Olivecrona, G. and Ryan, R.O. (2005) Apolipoprotein A-V-heparin interactions: implications for plasma lipoprotein metabolism. *J. Biol. Chem.,* **280,** 25383-25387.
14. Mullick, A.E., Deckelbaum, R.J., Goldberg, I.J., Al-Haideri, M. and Rutledge, J.C. (2002) Apolipoprotein E and lipoprotein lipase increase triglyceride-rich particle binding but decrease particle penetration in arterial wall. *Arterioscler. Thromb. Vasc. Biol.,* **22,** 2080–2085.
15. Olivecrona, T., Bengtsson-Olivecrona, G., Marklund, S.E., Lindahl, U. and Hook, M. (1977) Heparin-lipoprotein lipase interactions. *Fed. Proc.,* **36,** 60–65.
16. Lookene, A., Groot, N.B., Kastelein, J.J., Olivecrona, G. and Bruin, T. (1997) Mutation of tryptophan residues in lipoprotein lipase. Effects on stability, immunoreactivity, and catalytic properties. *J. Biol. Chem.,* **272,** 766–72.
17. Merkel, M., Kako, Y., Radner, H., Cho, I.S., Ramasamy, R., Brunzell, J.D., Goldberg, I.J. and Breslow, J.L. (1998) Catalytically inactive lipoprotein lipase expression in muscle of transgenic mice increases very low density lipoprotein uptake: Direct evidence that lipoprotein lipase bridging occurs *in vivo*. *Proc. Natl. Acad. Sci. USA,* **95,** 13841–13846.
18. Moore, K.L., Lombi, E., Zhao, F.-J. and Grovenor, C.R.M. (2012) Elemental imaging at the nanoscale: NanoSIMS and complementary techniques for element localisation in plants. *Anal. Bioanal. Chem,* **402,** 3263–3273.
19. Reitsma, S., Slaaf, D.W., Vink, H., van Zandvoort, M.A.M.J. and oude Egrink, M.G.A. (2007) The endothelial glycocalyx: composition, functions, and visualization. *Pfugers Arch. Eur. J. Physiol.,* **454,** 345–359.
20. Arkill, K.P., Neal, C.R., Mantell, J.M., Michel, C.C., Qvortrup, K., Rostgaard, J., Bates, D.O., Knupp, C. and Squire, J.M. (2012) 3D reconstruction of the glycocalyx structure in mammalian capillaries using electron tomography. *Microcirculation,* **19,** 343–351.
21. Mastronarde, D.N. (1997) Dual-axis tomography: an approach with alignment methods that preserve resolution. *J. Struct. Biol.,* **120,** 343–352.

22. Robertson, J.D. (1960) The molecular structure and contact relationships of cell membranes. *Prog. Biophys. Mol. Biol.,* **10,** 343–418.

23. Sonnenburg, W.K., Yu, D., Lee, E.C., Xiong, W., Gololobov, G., Key, B., Gay, J., Wilganowski, N., Hu, Y., Zhao, S. *et al.* (2009) GPIHBP1 stabilizes lipoprotein lipase and prevents its inhibition by angiopoietin-like 3 and angiopoietin-like 4. *J. Lipid Res.,* **50,** 2421–2429.

24. Lichtenstein, L., Mattijssen, F., de Wit, N.J., Georgiadi, A., Hooiveld, G.J., van der Meer, R., He, Y., Qi, L., Koster, A., Tamsma, J.T. *et al.* (2010) Angptl4 protects against severe pro-inflammatory effects of dietary saturated fat by inhibiting lipoprotein lipase-dependent uptake of fatty acids in mesenteric lymph node macrophages. *Cell Metab.,* **12,** 580–592.

25. Gin, P., Beigneux, A.P., Voss, C., Davies, B.S., Beckstead, J.A., Ryan, R.O., Bensadoun, A., Fong, L.G. and Young, S.G. (2011) Binding preferences for GPIHBP1, a glycosylphosphatidylinositol-anchored protein of capillary endothelial cells. *Arterioscler. Thromb. Vasc. Biol.,* **31,** 176-182.

26. Liu, M.S., Ma, Y., Hayden, M.R. and Brunzell, J.D. (1992) Mapping of the epitope on lipoprotein lipase recognized by a monoclonal antibody (5D2) which inhibits lipase activity. *Biochim. Biophys. Acta,* **1128,** 113-115.

27. Chang, S.-F., Reich, B., Brunzell, J.D. and Will, H. (1998) Detailed characterization of the binding site of the lipoprotein lipase-specific monoclonal antibody 5D2. *J. Lipid Res.,* **39,** 2350-2359.

28. Olafsen, T., Young, S.G., Davies, B.S., Beigneux, A.P., Kenanova, V.E., Voss, C., Young, G., Wong, K.P., Barnes, R.H., 2nd, Tu, Y. *et al.* (2010) Unexpected expression pattern for glycosylphosphatidylinositol-anchored HDL-binding protein 1 (GPIHBP1) in mouse tissues revealed by positron emission tomography scanning. *J. Biol. Chem.,* **285,** 39239-39248.

29. Garcia-Arcos, I., Hiyama, Y., Drosatos, K., Bharadwaj, K.G., Hu, Y., Son, N.H., O'Byrne, S.M., Chang, C.L., Deckelbaum, R.J., Takahashi, M. *et al.* (2013) Adipose-specific lipoprotein lipase deficiency more profoundly affects brown than white fat biology. *J. Biol. Chem.,* **288,** 14046–14058.

30. Levak-Frank, S., Weinstock, P.H., Hayek, T., Verdery, R., Hofmann, W., Ramakrishnan, R., Sattler, W., Breslow, J.L. and Zechner, R. (1997) Induced mutant mice expressing lipoprotein lipase exclusively in muscle have subnormal triglycerides yet reduced high density lipoprotein cholesterol levels in plasma. *J. Biol. Chem.,* **272,** 17182–17190.

31. Wang, L., Fuster, M., Sriramarao, P. and Esko, J.D. (2005) Endothelial heparan sulfate deficiency impairs L-selectin- and chemokine-mediated neutrophil trafficking during inflammatory responses. *Nature Immunol.,* **6,** 902–910.

32. Grobe, K., Ledin, J., Ringvall, M., Holmbom, K., Forsberg, E., Esko, J.D. and Kjellen, L. (2002) Heparan sulfate and development: differential roles of

the N-acetylglucosamine N-deacetylase/N-sulfotransferase isozymes. *Biochem. Biophys. Acta,* **1573,** 209–215.

33. Takahashi, M., Hiyama, Y., Yokoyama, M., Yu, S., Hu, Y., Melford, K., Bensadoun, A. and Goldberg, I.J. (2008) In vivo arterial lipoprotein lipase expression augments inflammatory responses and impairs vascular dilatation. *Arterioscler. Thromb. Vasc. Biol.,* **28,** 455–462.

34. Weinstein, M.M., Yin, L., Beigneux, A.P., Davies, B.S.J., Gin, P., Estrada, K., Melford, K., Bishop, J.R., Esko, J.D., Dallinga-Thie, G.M. *et al.* (2008) Abnormal patterns of lipoprotein lipase release into the plasma in GPIHBP1-deficient mice. *J. Biol. Chem.,* **283,** 34511–34518.

35. Bartelt, A., Bruns, O.T., Reimer, R., Hohenberg, H., Ittrich, H., Peldschus, K., Kaul, M.G., Tromsdorf, U.I., Weller, H., Waurisch, C. *et al.* (2011) Brown adipose tissue activity controls triglyceride clearance. *Nat. Med.,* **17,** 200–205.

36. Wong, H., Yang, D., Hill, J.S., Davis, R.C., Nikazy, J. and Schotz, M.C. (1997) A molecular biology-based approach to resolve the subunit orientation of lipoprotein lipase. *Proc. Natl. Acad. Sci. USA,* **94,** 5594–5598.

37. Kobayashi, Y., Nakajima, T. and Inoue, I. (2002) Molecular modeling of the dimeric structure of human lipoprotein lipase and functional studies of the carboxy-terminal domain. *Eur. J. Biochem.,* **269,** 4701–4710.

38. Blanchette-Mackie, E.J., Masuno, H., Dwyer, N.K., Olivecrona, T. and Scow, R.O. (1989) Lipoprotein lipase in myocytes and capillary endothelium of heart: Immunocytochemical study. *Am. J. Physiol.,* **256,** E818–E828.

39. Moore, D.H. and Ruska, H. (1957) The fine structure of capillaries and small arteries. *J. Biophys, and Biochem. Cytol.,* **3,** 457–475.

FIGURE LEGENDS

Fig. 1. Binding of triglyceride-rich lipoproteins (TRLs) to small blood vessels in the heart. (A) FITC-labeled lectin and Alexa555-labeled TRLs were mixed together and injected into a *Gpihbp1*$^{+/+}$ and *Gpihbp1*$^{-/-}$ mouse. The lectin binds to endothelial cells and is used to identify all blood vessels (green). TRLs (red) bound exclusively to small capillaries in the wild-type heart and were absent from larger blood vessels (see arrowhead). DAPI was used to visualize nuclei (blue). (B) High-magnification confocal fluorescence microscopy images showing TRL binding in the lumen of a capillary. A wild-type mouse was injected with Alexa555-labeled TRLs (red), and after 30 sec, unbound lipoproteins were removed by perfusion. Heart sections were stained with antibodies against GPIHBP1 (green) and CD31 (magenta), a marker of endothelial cells, and DAPI to visualize nuclei (blue). (C) Transmission EM showing numerous TRLs along the luminal surface of capillaries in the *Gpihbp1*$^{+/+}$ heart but none in capillaries of the *Gpihbp1*$^{-/-}$ heart. In the wild-type heart capillary, there were a few lipoproteins that appeared separated from the endothelial cell surface (arrow). Scale bar, 200 nm. (D) NanoSIMS analysis showing TRL binding to capillary endothelial cells in the heart. A wild-type mouse was injected with ^{13}C-labeled TRLs, and after 8 min was perfused with PBS to remove unbound lipoproteins. Heart tissue sections were analyzed by nanoSIMS and back-scattered electron (BSE) imaging. The ^{13}C-signal was normalized to the ^{12}C-signal. A ^{13}C/^{12}C-signal in the natural abundance range appears blue, whereas an increased ^{13}C/^{12}C-signal appears yellow–red. Areas of ^{13}C/^{12}C enrichment corresponded to TRLs at the capillary lumen (detected by high-resolution BSE imaging on the same sections; arrows).

Fig. 2. Alcian blue staining and dual-axis electron microscopy tomography of hearts from mice showing TRL binding inbetween patches of glycocalyx. Unlabeled TRLs were injected into wild-type mice. After 30 sec, the mice were perfused with PBS to remove unbound lipoproteins, followed immediately with glutaraldehyde fixative containing Alcian blue to stain the glycocalyx. Embedded heart tissues were sectioned and examined by dual-axis electron tomography. TRLs bind to gaps inbetween patches of glycocalyx. Higher-magnification images of the boxed areas are shown in the lower panels. Note the close apposition of the TRLs with the endothelial cell plasma membrane. Scale bar, 800 nm. The complete tomogram can be viewed in Videos S1–S3.

Fig. 3. Dual-axis electron microscopy tomography of hearts from mice injected with TRLs. Unlabeled TRLs were injected into a wild-type mouse. After 30 sec, the mouse was perfused with PBS to remove unbound lipoproteins. **(**A–C) TRLs on the surface of capillary endothelial cells were in many cases attached to thin membrane structures protruding from the luminal surface of endothelial cells—which we have called nanovilli (NV). Nanovilli were also observed within intracellular vesicles (D–F) and at the basolateral plasma membrane (E). Scale bar, 70 nm. Nanovilli had the “railroad-track” morphology of lipid bilayers (F). Immunogold EM studies to determine the subcellular localization of GPIHBP1. We found many instances of linear arrays of gold particles extending into the capillary lumen or within intracellular vesicles (arrows) (G–I). Scale bar, 100 nm. For panels A–F, see also Videos S4–S6.

Fig. 4. The binding of TRLs in the heart is dependent on GPIHBP1 expression. IR800-dye–labeled TRLs (green) and IR680-dye–labeled β-VLDL

(red) were mixed together and injected into a *Gpihbp1*$^{+/+}$ and a *Gpihbp1*$^{-/-}$ mouse. After 30 sec, the mice were perfused with PBS to remove unbound lipoproteins, followed immediately by fixative. Tissue sections (10-μm thick) were scanned on an Odyssey infrared imager, and the amounts of TRL and β-VLDL binding were measured and normalized to tissue area. (A) Images of tissue sections from the heart, brain, liver, and brown adipose tissue (BAT) showing TRL binding in the heart in *Gpihbp1*$^{+/+}$ but not *Gpihbp1*$^{-/-}$ mice. (C) Images of the same tissue sections showing β-VLDL (red) binding, which was mainly in the liver. Quantification of TRL and β-VLDL binding is shown in panels B and D, respectively.

Fig. 5. Immunofluoresence microscopy showing that the binding of TRLs and lipid emulsions (Intralipid) to cells depends on the carboxyl-terminal lipid-binding domain of LPL. CHL-11 cells were transfected with empty vector or S-protein–tagged GPIHBP1. The cells were incubated with V5-tagged human LPL (h-LPL) in the absence or presence of antibody 5D2, a mouse monoclonal antibody that blocks the lipid-binding domain of LPL (27), or a mouse monoclonal antibody against the V5-protein tag. After washing the cells, the cells were incubated with (A) DiI-labeled TRLs (red) or (B) DiI-labeled Intralipid at 4° C, and the binding determined by fluorescence microscopy. GPIHBP1 expression (green) and LPL binding (magenta) were determined with specific antibodies. Nuclei were stained with DAPI (blue). Images were recorded on an Axiovert 200M microscope with a 20× objective.

Fig. 6. Binding of TRLs in the lung and heart is dependent on both GPIHBP1 and LPL. (A) Wild-type and *Gpihbp1* knockout mice were injected

intravenously with bovine LPL (65 µg in saline) or saline alone, followed by IR800-dye–labeled TRLs (green). After 30 sec, the mice were perfused with PBS to remove unbound lipoproteins, and the amount of TRL binding determined by infrared scanning. In saline injected animals, TRL binding (green) was detected in the heart of the wild-type mouse but very little in the *Gpihbp1*$^{-/-}$ mouse. TRL binding in the lung was negligible for both the wild-type and *Gpihbp1*$^{-/-}$ mouse. After the injection of bLPL (+bLPL), there was a substantial increase in TRL binding in the lung of wild-type mice, but not in the *Gpihbp1*$^{-/-}$ mouse. The results normalized to tissue area are shown in the bar graph. (B) IR800-dye–labeled TRLs (green) were injected into wild-type (WT), *Gpihbp1*$^{-/-}$ (GpiKO), or *Lpl*$^{-/-}$ mice expressing a human *LPL* transgene in muscle ("L0-MCK"). In another group of L0-MCK mice, a monoclonal antibody against human LPL (5D2) was injected 3 min before the injection of TRLs. After 30 sec, the amount of TRL binding was measured as described in A (with the WT set at a value of one). Representative images of heart tissue sections are shown in the insets. The anti-human LPL antibody reduced TRL binding in the hearts of L0-MCK mice to levels observed in *Gpihbp1*$^{-/-}$ mice. The same antibody had no effect on TRL binding in wild-type mice (Fig. S7B).

Fig. 7. LPL produced directly by endothelial cells is unable to increase the binding of TRLs in *Gpihbp1* knockout mice. Wild-type (WT), *Gpihbp1*$^{-/-}$, and *Gpihbp1*$^{-/-}$ mice expressing human LPL from an endothelial cell–specific *LPL* transgene (*Gpihbp1*$^{-/-}$EC-*hLPL*) were injected with IR800-dye–labeled TRLs and IR680-dye–labeled lectin. After 30 sec, the mice were perfused with PBS to remove unbound materials, and the amounts of TRL and lectin binding were measured by infrared scanning. The expression of human LPL in endothelial

cells increased preheparin plasma LPL levels more than 8-fold and reduced plasma triglyceride levels by more than 90% (for panel A, triglycerides were 3192 mg/dl *vs.* 301 mg/dl; for panel B, triglycerides were 3968 mg/dl *vs.* 231 mg/dl). Quantitative analyses showed that LPL synthesized and secreted by endothelial cells did not increase TRL binding in the heart. Representative images of heart tissue sections from wild-type (WT), *Gpihbp1*$^{-/-}$ (KO), and *Gpihbp1*$^{-/-}$EC-*hLPL* (KOT) mice are shown in the insets.

Figure 1
Click here to download high resolution image

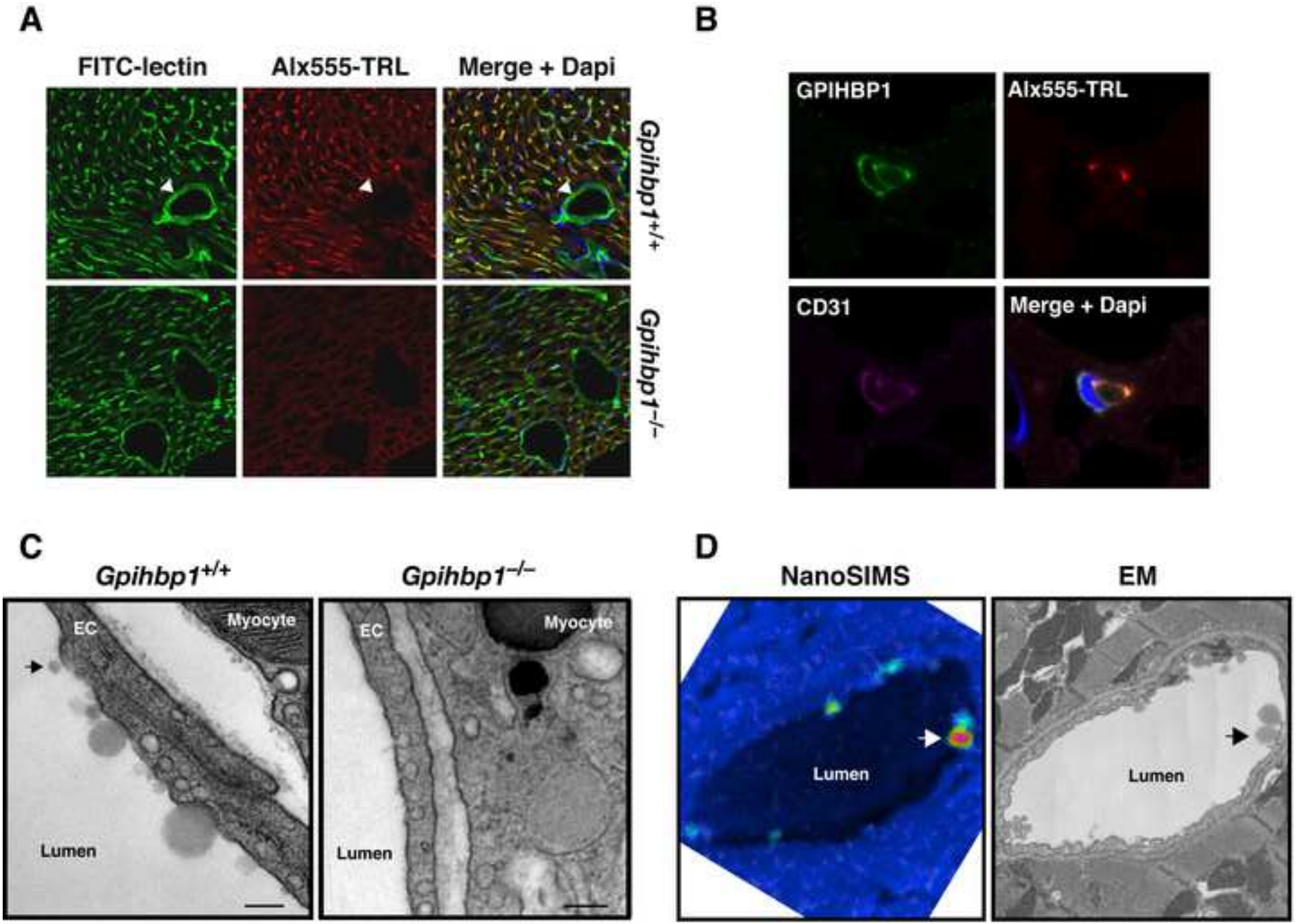

Figure 2
Click here to download high resolution image

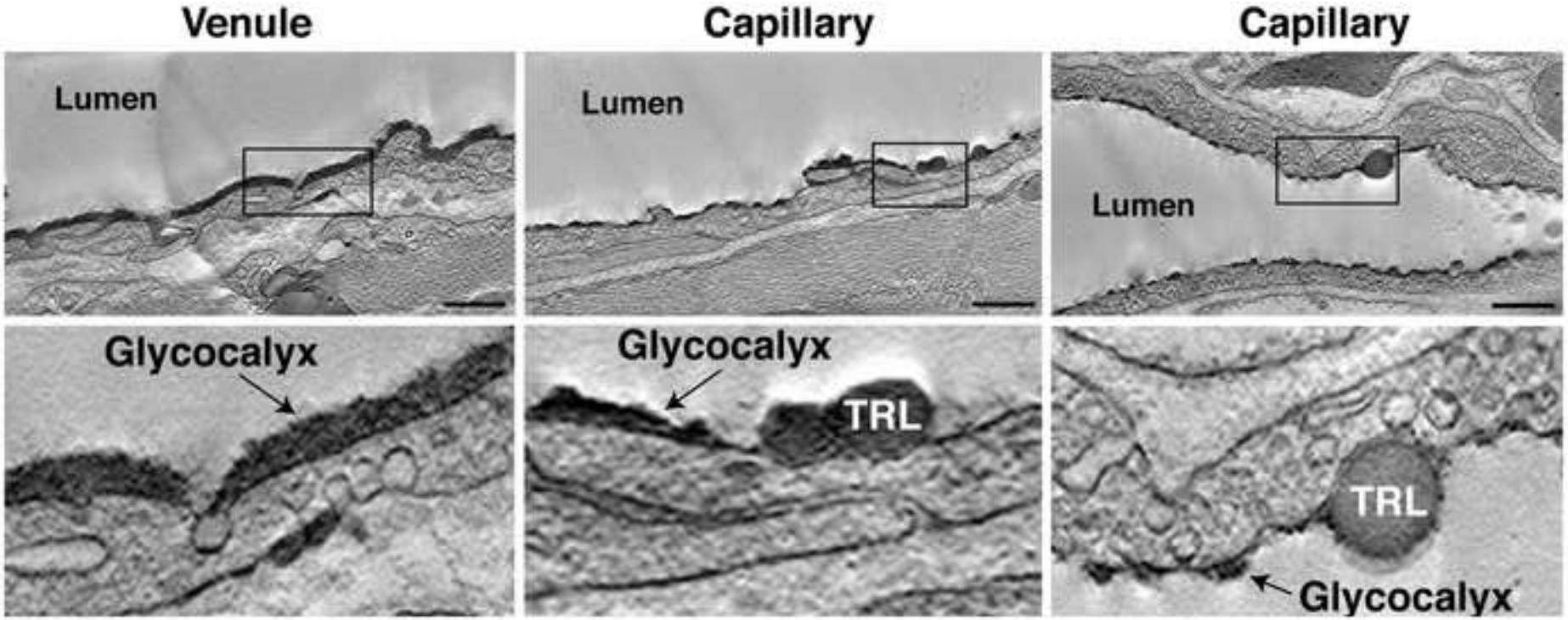

Figure 3
Click here to download high resolution image

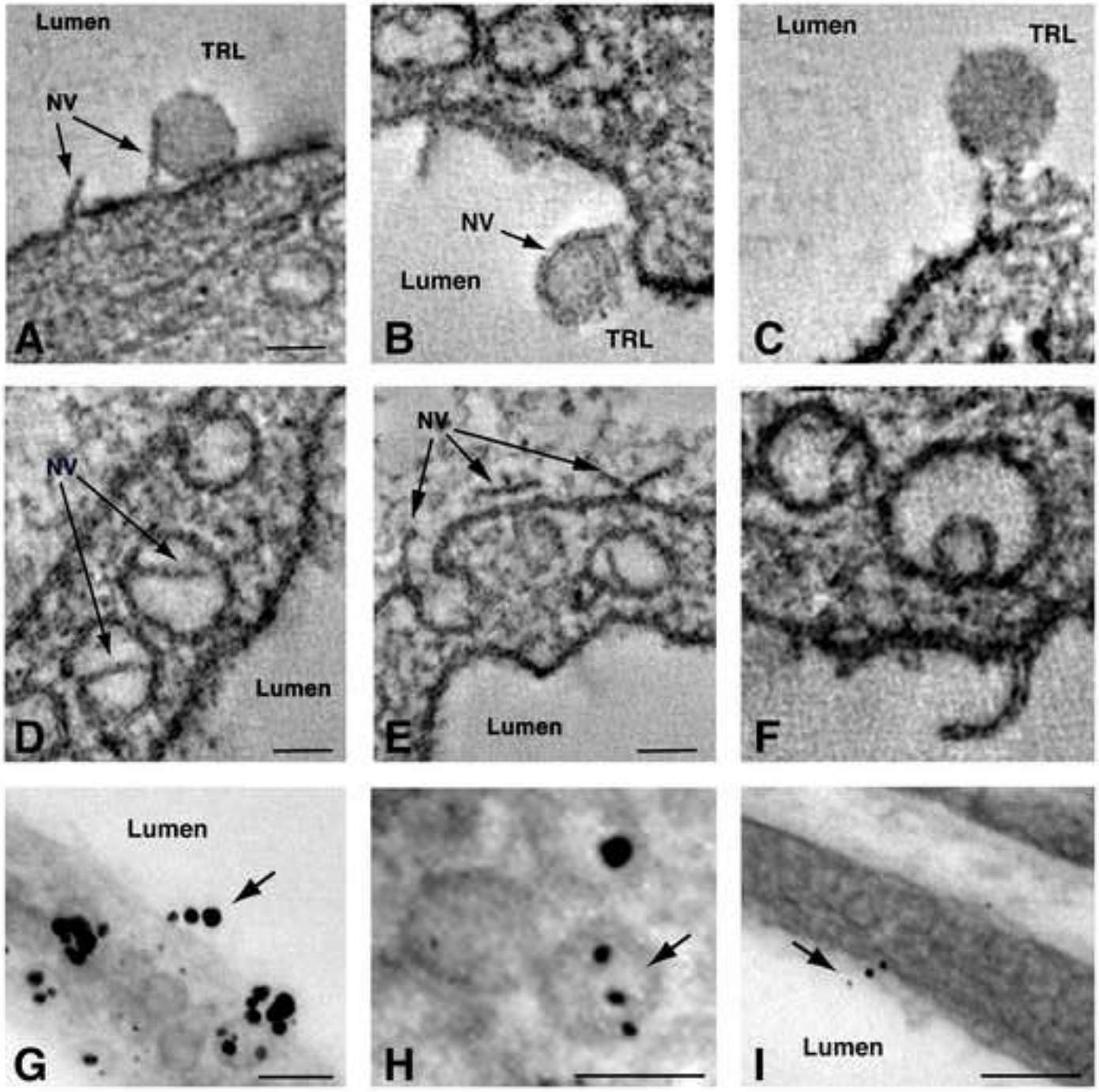

Figure 4
Click here to download high resolution image

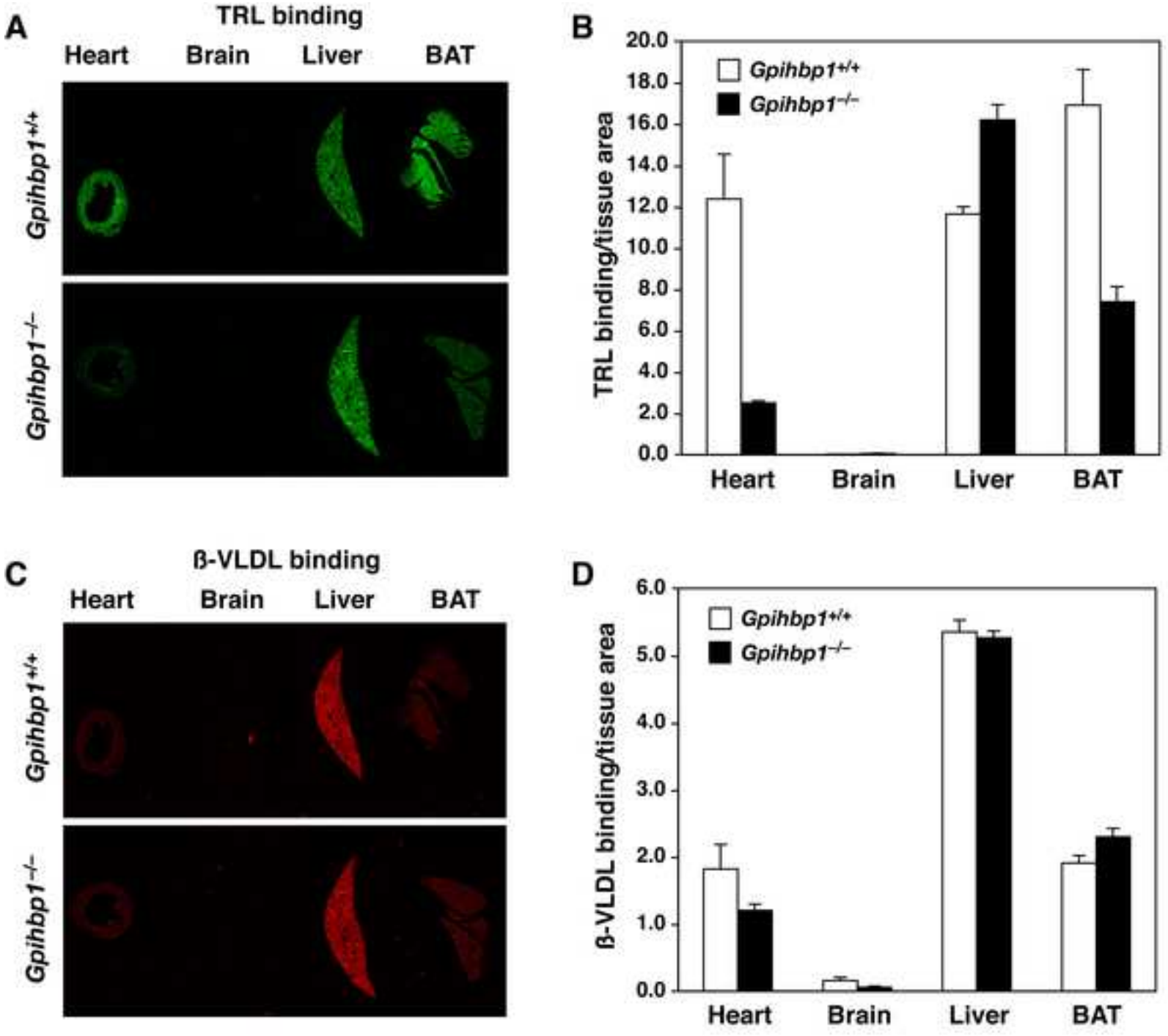

Figure 5
Click here to download high resolution image

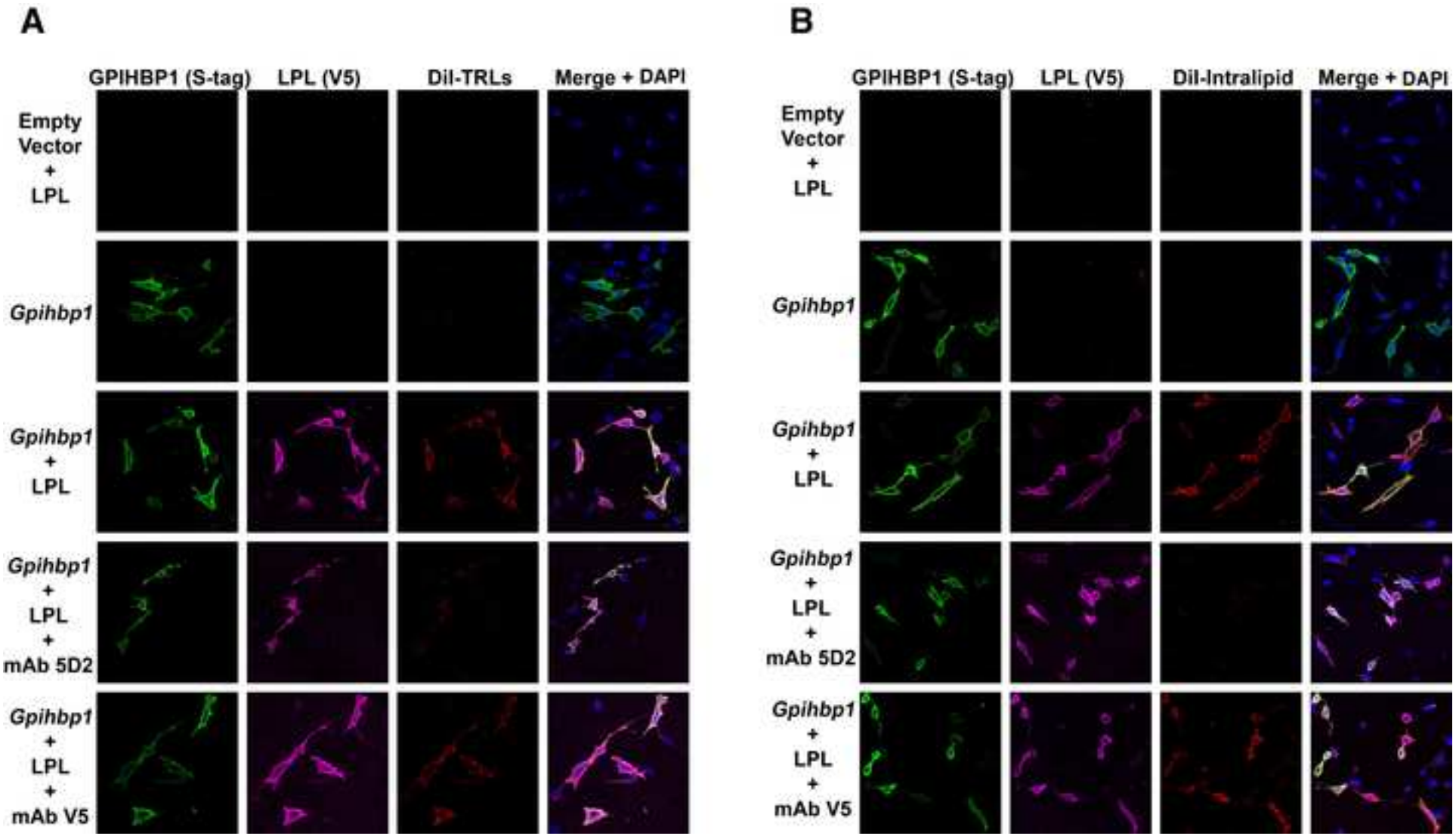

Figure 6
Click here to download high resolution image

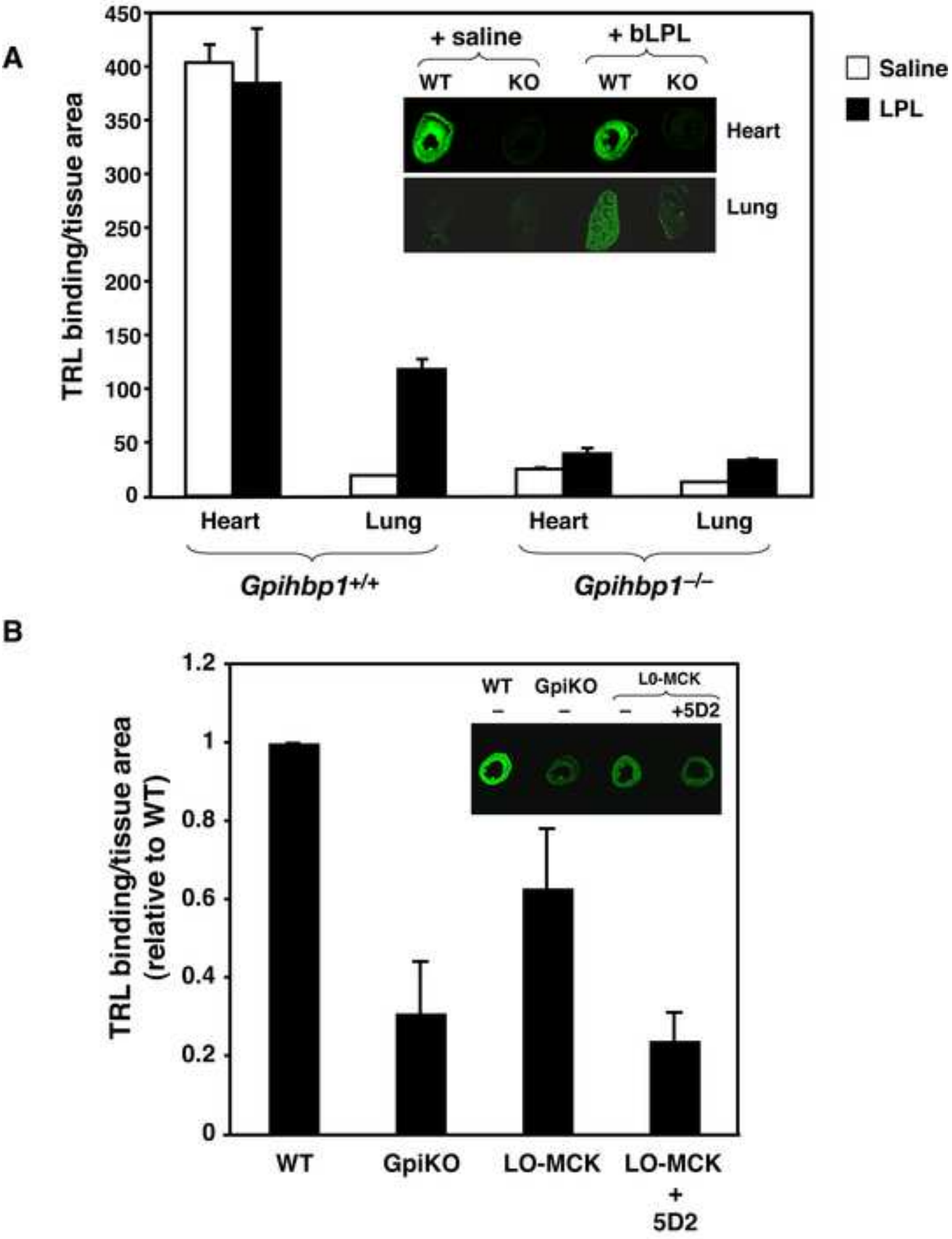

Figure 7
Click here to download high resolution image

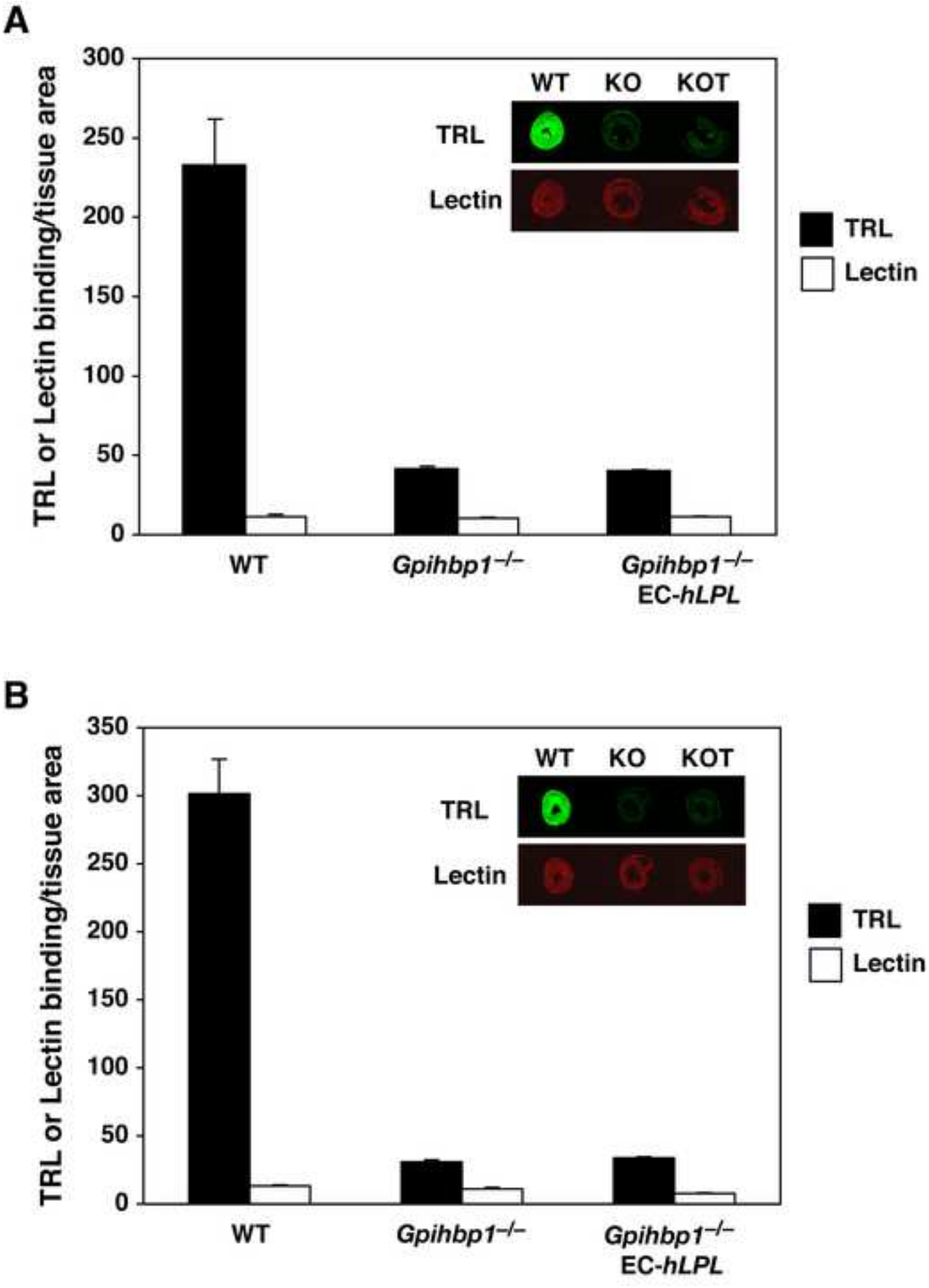

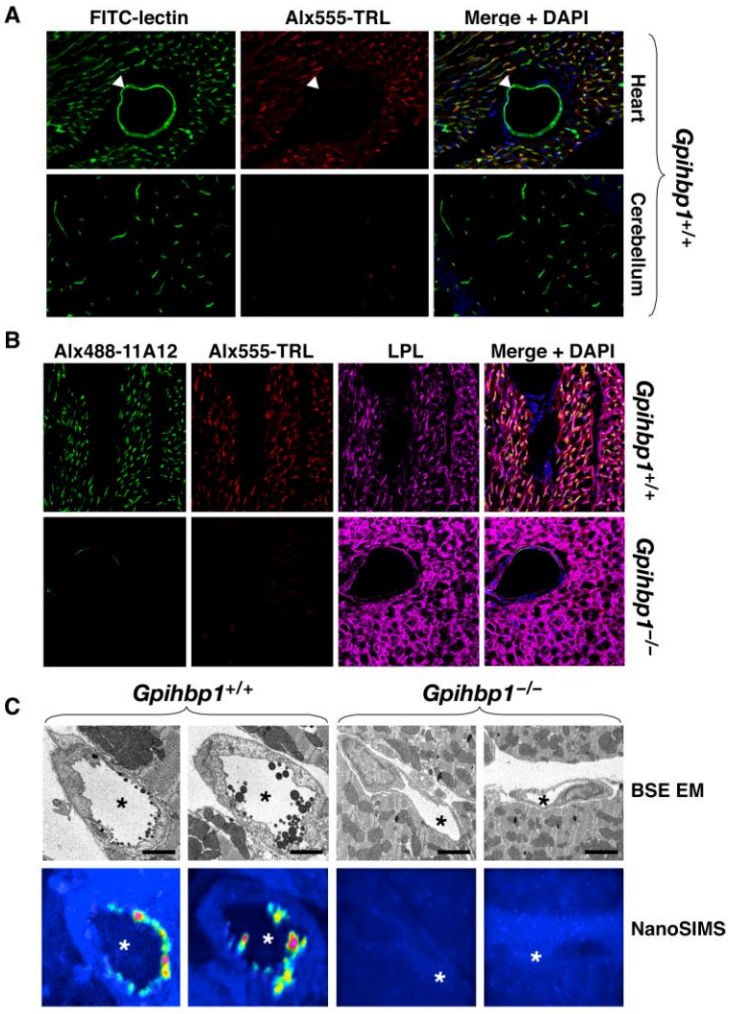

Figure S1. Triglyceride-rich lipoprotein (TRL) binding parallels GPIHBP1 expression. Related to Figure 1. (A) Fluorescence microscopy images showing TRL binding (red) in small blood vessels (green) but absent in large blood vessels (arrowhead), and in the cerebellum, a tissue that does not express GPIHBP1 (1). (B) Fluorescence microscopy images showing that TRL binding (red) closely matched the staining patterns for GPIHBP1 (green) and LPL (magenta) in the heart of a wild-type mouse. (C) NanoSIMS analysis showing TRL binding to capillary endothelial cells in a wild-type mouse but not in a *Gpihbp1*$^{-/-}$ mouse. Capillary lumens are identified with an asterisk.

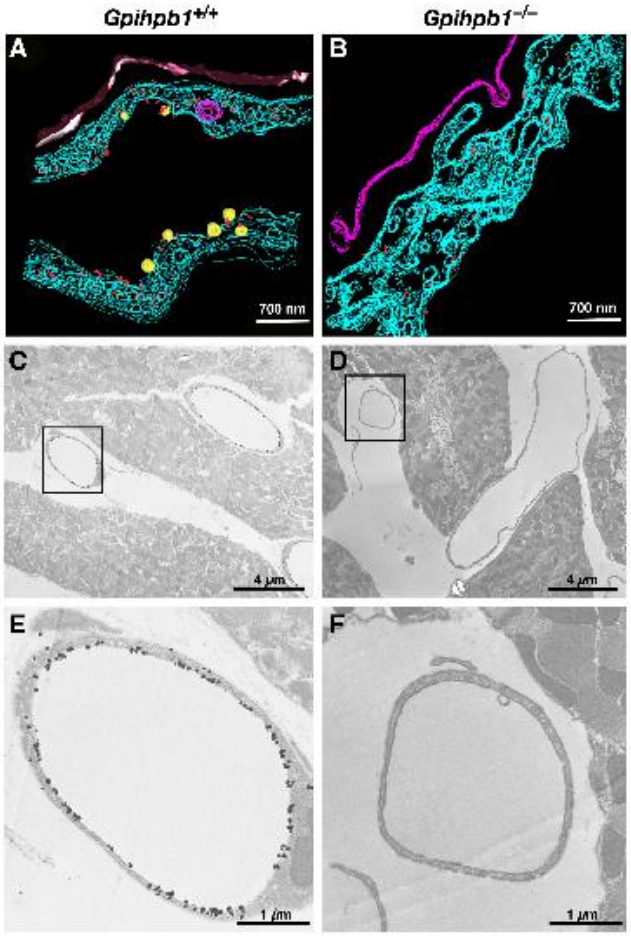

Figure S2. Distribution of nanovilli, TRL binding, and GPIHBP1 expression in heart capillaries. Related to Figure 3. (A, B) 3-D modeling of 131 individual EM tomograms revealed multiple TRLs attached to the endothelial cell surface in *Gpihbp1*$^{+/+}$ but not *Gpihbp1*$^{-/-}$ mice. Contour lines were drawn to outline TRLs (yellow), myocytes (magenta), endothelial cell membranes (blue), and nanovilli (red), on endothelial cells. (C, D) Low-magnification and (E, F) high-magnification transmission EM images showing many gold particles (GPIHBP1) in capillaries of the wild-type mouse (C, E) but none in the *Gpihbp1*$^{-/-}$ mouse (D, F). The boxed areas in panels C and D are shown at higher magnification in panels E and F, respectively.

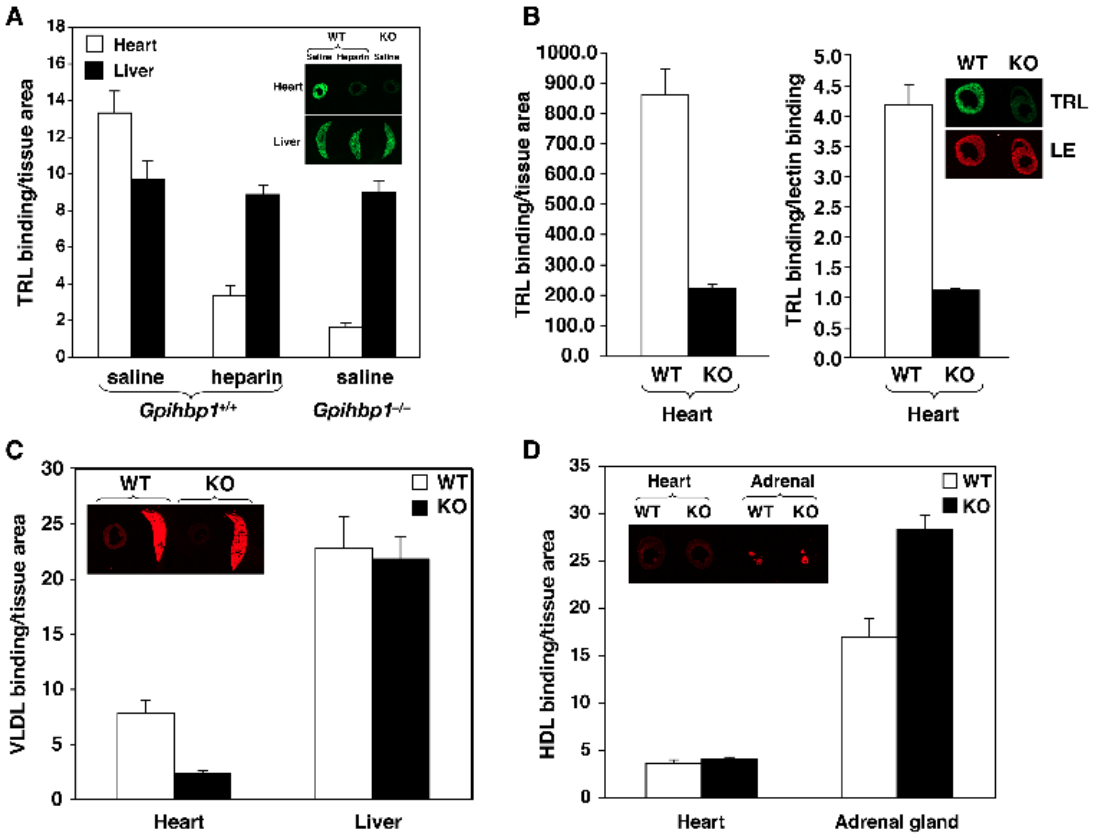

Figure S3. The margination of TRLs in the heart is heparin-sensitive, dependent on GPIHBP1 expression, and specific. Related to Figure 4. (A) Heparin (100 U) reduced the amount of TRL binding in wild-type mice to levels observed in saline-injected *Gpihbp1*$^{-/-}$ mice. (B) TRL binding was lower in *Gpihbp1*$^{-/-}$ hearts than in wild-type mouse hearts after normalization to tissue area (left) or endothelial cell content as judged by lectin (LE) binding (right). (C) The binding of both TRLs (not shown) and human VLDL in the heart was lower in *Gpihbp1* knockout mice (reduced by 71% for VLDL and 72% for TRLs). (D) HDL binding was very low in the heart but high in the adrenal gland. The absence of GPIHBP1 did not reduce HDL binding in either tissue.

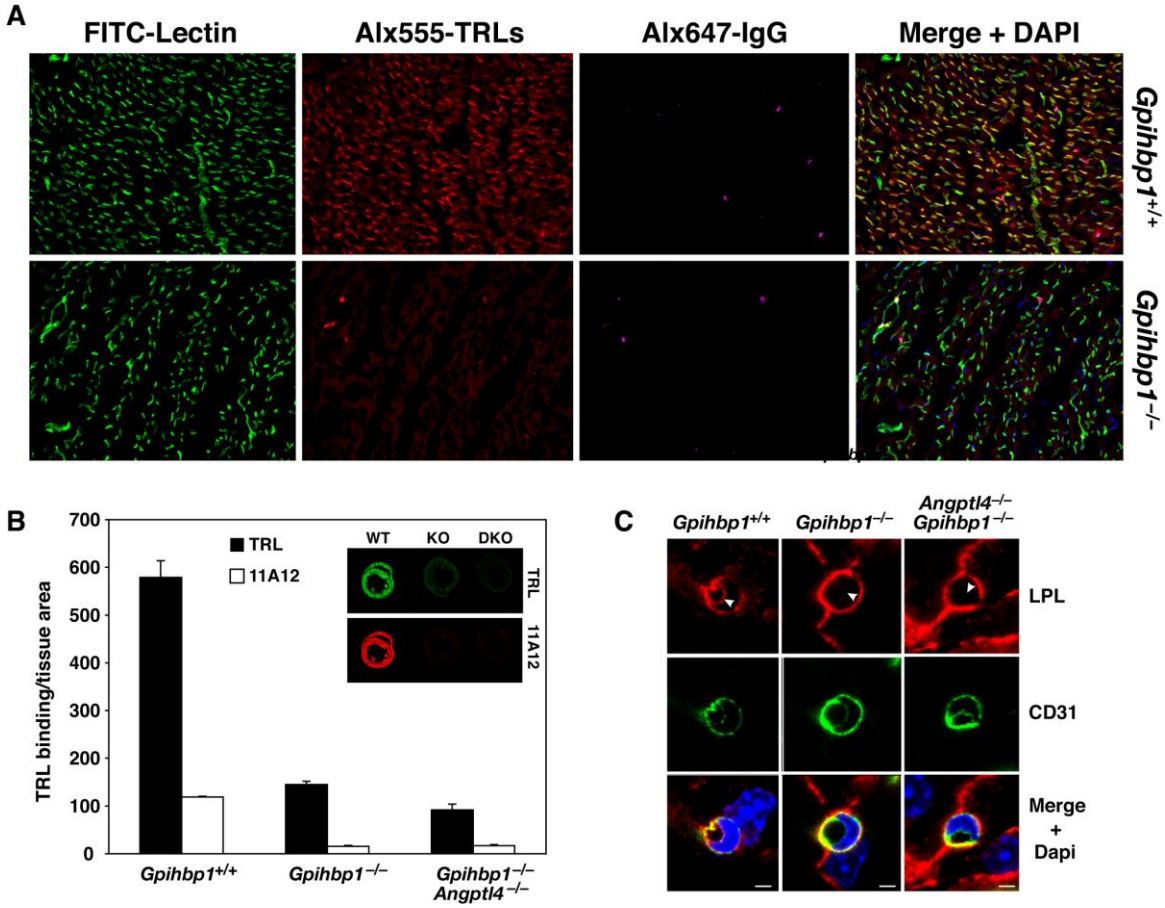

Figure S4. The reduced binding of TRLs in *Gpihbp1*$^{-/-}$ mouse hearts is not due to high plasma triglyceride levels. Related to Figure 4. (A) Isolated hearts from *Gpihbp1*$^{+/+}$ and *Gpihbp1*$^{-/-}$ mice were cannulated and perfused with FITC-labeled lectin (green), Alexa555-labeled TRLs (red), and Alexa647-labeled rat IgG. TRL binding was detected in wild-type hearts and colocalized with endothelial cells. The binding was eliminated when heparin was included in the perfusion solution (not shown). In *Gpihbp1*$^{-/-}$ mice, TRL binding was low. There were areas that were "positive" for TRLs, but those coincided with areas of incomplete perfusion, as judged by Alexa647-IgG staining (magenta). (B) ANGPTL4 deficiency does not increase TRL binding in *Gpihbp1*$^{-/-}$ mice. *Angptl4*-deficiency has been reported to reduce plasma triglyceride levels in *Gpihbp1*$^{-/-}$ mice (2). In our studies, fasting plasma triglyceride levels were 1742 mg/dl in

Gpihbp1$^{-/-}$ mice *vs*. 132 mg/dl in *Gpihbp1*$^{-/-}$*Angptl4*$^{-/-}$ mice. However, the margination of IR-dye–labeled TRLs was not greater in heart capillaries of *Gpihbp1*$^{-/-}$*Angptl4*$^{-/-}$ mice. (C) Confocal fluorescence microscopy images of cross sections through an endothelial cell nucleus, stained with DAPI (blue), were captured on a confocal microscope with a 63× objective and 3× optical zoom. LPL (green) was absent from the luminal face of endothelial cells in both *Gpihbp1*$^{-/-}$ and *Gpihbp1*$^{-/-}$*Angptl4*$^{-/-}$ mice. The locations of the capillary lumens are identified with arrowheads.

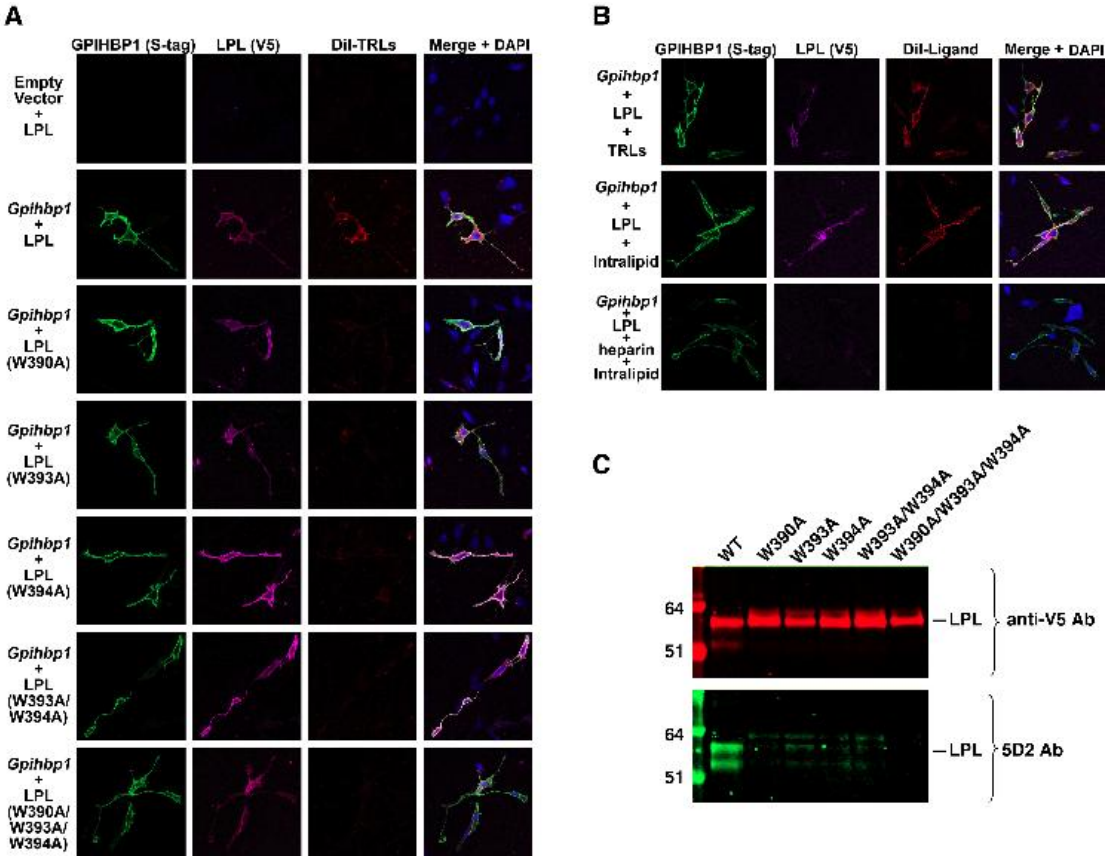

Figure S5. Immunofluoresence microscopy showing that the binding of TRLs to GPIHBP1-bound LPL depends on a cluster of tryptophans in LPL's carboxyl-terminal domain and that the binding of Intralipid to GPIHBP1-bound LPL is sensitive to heparin. Related to Figure 5. (A) CHL-11 cells were transfected with GPIHBP1 (green) and the binding of DiI-labeled TRLs (red) measured after the addition of wild-type LPL or different LPL mutants (as indicated) (magenta). TRLs only bound to cells that had wild-type LPL on their cell surface. (B) The binding of DiI-labeled Intralipid particles (red) to GPIHBP1-expressing cells (green) incubated with wild-type LPL (magenta) was blocked by heparin. (C) Western blot analysis showing that mutagenesis of the tryptophan cluster in the carboxyl terminus of LPL inhibits antibody 5D2 binding.

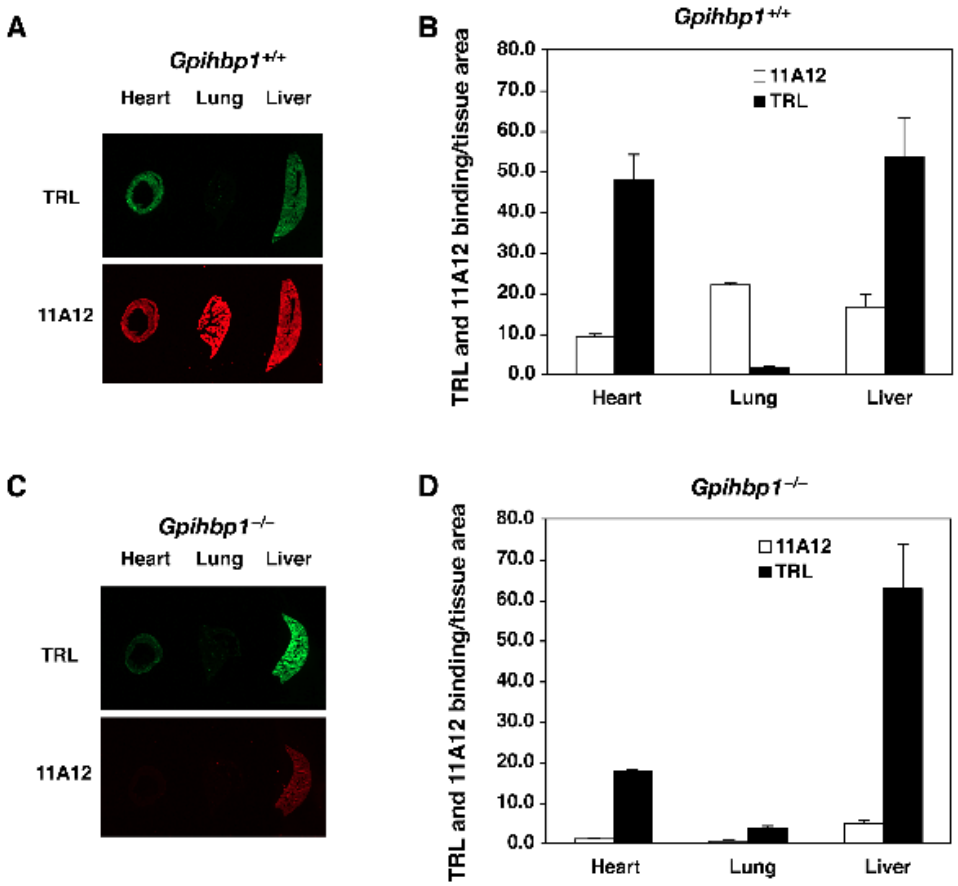

Figure S6. TRLs bind poorly in the lung despite high levels of GPIHBP1 expression. Related to Figure 6. (A, B) Images of representative tissue sections, and quantitative data showing high GPIHBP1 expression (as detected by antibody 11A12, red) but very low levels of TRL binding (green) in the lungs of wild-type mice. (C, D) Images of representative tissue sections, and quantitative data showing very little antibody 11A12 binding or TRL binding in the lungs of *Gpihbp1*$^{-/-}$ mice.

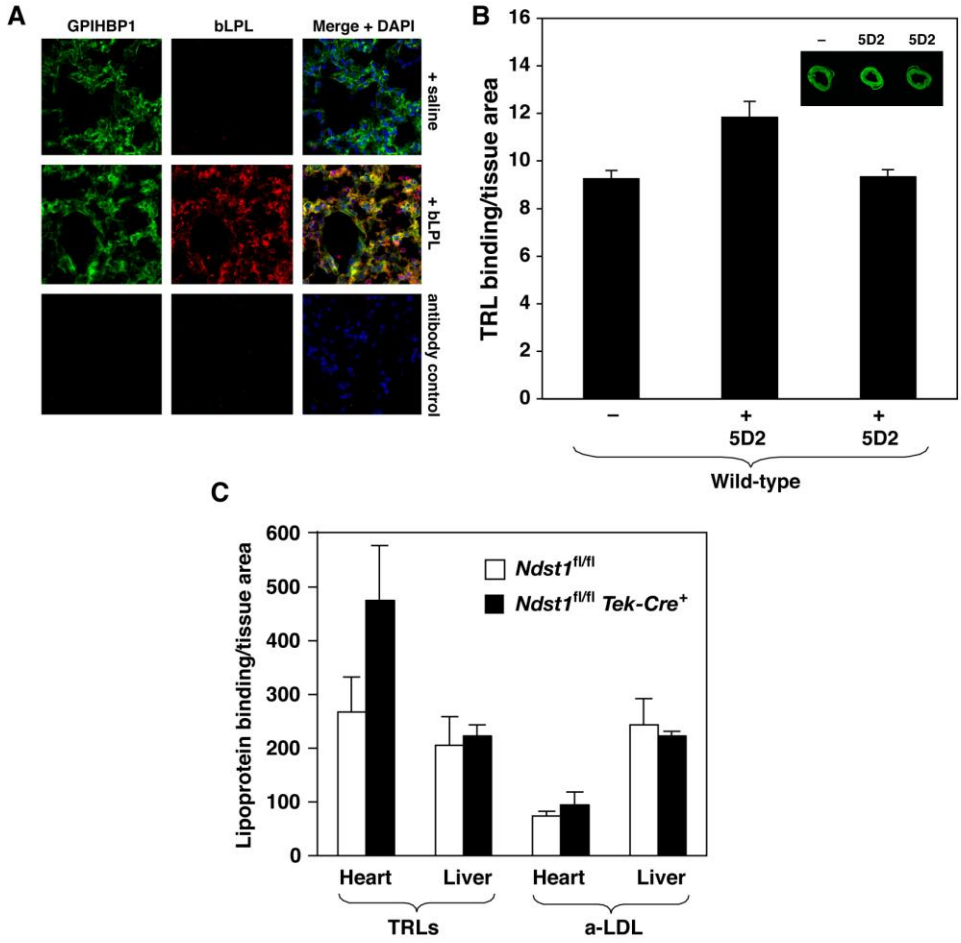

Figure S7. Bovine LPL, when injected intravenously, is captured by capillaries of the lung of wild-type mice. Inhibition of HSPG sulfation does not inhibit TRL margination in the heart. Related to Figures 6 & 7. (A) Immunofluorescence microscopy images showing the capture of injected bovine LPL (red) by endothelial cells in the lung. (B) Quantitative measurements showing that antibody 5D2 does not reduce TRL binding in wild-type mice. Representative image of heart tissue sections is shown in the inset. (C) Quantitative analyses showing that *Ndst1*-deficiency does not reduce TRL or a-LDL binding in the heart (or liver).

LEGENDS FOR SUPPLEMENTAL MOVIES

Movie S1. Movie showing a dual-axis electron microscopy tomogram of a capillary from a wild-type mouse injected with triglyceride-rich lipoproteins and stained with Alcian blue. Related to figure 2.

Movie S2. Movie showing a dual-axis electron microscopy tomogram of a capillary from a wild-type mouse injected with triglyceride-rich lipoproteins and stained with Alcian blue. Related to figure 2.

Movie S3. Movie showing a dual-axis electron microscopy tomogram of a venule from a wild-type mouse injected with triglyceride-rich lipoproteins and stained with Alcian blue. Related to figure 2.

Movie S4. Movie showing a dual-axis electron microscopy tomogram of a heart from a wild-type mouse injected with triglyceride-rich lipoproteins. Related to figures 3 and S2.

Movie S5. Movie showing a close-up view of a triglyceride-rich lipoprotein particle attached to a nanovillus on the surface of a heart capillary endothelial cell. Related to figures 3 and S2.

Movie S6. Movie showing a close-up view of multiple nanovilli within invaginations and vesicles of a heart capillary endothelial cell. Related to figures 3 and S2.

SUPPLEMENTAL EXPERIMENTAL PROCEDURES

Animal models. *Gpihbp1*$^{-/-}$ (3), *Angptl4*$^{-/-}$ (4), *Ndst1*$^{fl/fl}$*Tek-Cre*$^{+}$ (5), L0-MCK mice (*Lpl*$^{-/-}$ mice harboring a muscle-specific human *LPL* transgene) (6), and EC-hLpLH mice (mice expressing a human *LPL* minigene driven by the Tie2 promoter) (7), have been described previously. Mice were fed a chow diet and housed in a barrier facility with a 12-h light-dark cycle. Triglyceride levels were measured on plasma samples with the Serum Triglyceride Determination Kit (Sigma). All studies were approved by UCLA's Animal Research Committee.

Isolation and labeling of lipoproteins. Triglyceride-rich lipoproteins (TRLs) were isolated from the plasma of *Gpihbp1*$^{-/-}$ mice by ultracentrifugation. Plasma (0.4 ml) was overlaid with PBS and centrifuged at 100,000 rpm (424,000 $\times$ *g*) at 10° C for 2 h in a Beckman TLA-100.3 rotor. The $d < 1.006$ g/dl lipoproteins were placed into a new tube, overlaid with PBS, and subjected to a second round of ultracentrifugation. The lipoproteins were removed and stored at 4° C. Cholesterol-rich very low density lipoproteins (β-VLDL) were isolated from the plasma of *Apoe*$^{-/-}$ mice after an overnight fast by ultracentrifugation. Human VLDL was purchased from Athens Research, and mouse HDL was isolated by ultracentrifugation (8). The apolipoproteins of TRLs as well as antibodies were labeled with infrared (IR) dyes (DyLight IR680-dye or DyLight IR800-dye) (Thermo Scientific). The proteins were diluted in PBS (2 mg/ml) containing 50 mM borate buffer (pH 8.5) and then incubated with the IR-dye for 1.5 h at RT with constant rotation. To separate labeled TRLs and antibodies from unincorporated dye, samples were applied to an Econo-Pac 10DG gel-filtration column (Bio-Rad). Lipoproteins and antibodies were also labeled with fluorescent dyes (Alexa488, Alexa555, Alexa647) (Invitrogen). The proteins were diluted in PBS (2

mg/ml) containing 100 mM bicarbonate buffer (pH 8.3) and incubated with the fluorescent dye for 1.5 h at RT with constant rotation. Again, the labeled proteins were separated from unincorporated dye by gel filtration. TRLs and Intralipid were also labeled with the fluorescent lipid dye 1,1′-dioctadecyl-3,3,3′,3′-tetramethylindocarbocyanine perchlorate (DiI; Invitrogen) for cell culture studies (the DiI-label was not suitable for *in vivo* studies). The dye was dissolved in DMSO (3 mg/ml), and 10 μl of this solution was added to TRLs or Intralipid along with lipoprotein-deficient human serum. DiI-labeled particles were isolated by density gradient ultracentrifugation.

Fluorescence microscopy. Tissues were perfusion fixed *in situ* with freshly prepared 3% paraformaldehyde (PFA) in PBS, and tissue samples were frozen in O.C.T. Tissue sections (8–10-μm thick) were processed for immunohistochemistry as described previously (1). GPIHBP1 was detected with the mouse GPIHBP1–specific rat monoclonal antibody 11A12 (mAb11A12) followed by Alexa488-labeled anti–rat IgG (1:200) or with Alexa555-labeled mAb11A12 (3 μg/ml). Endothelial cells were identified with a hamster anti-CD31 monoclonal antibody (1:200) and Alexa647-labeled anti–hamster IgG (1:200), or by injecting mice with FITC-labeled tomato lectin (100 μg). LPL was detected with a goat antibody against bovine LPL (1) and Alexa647-labeled anti–goat IgG. Nuclei were stained with DAPI. Images were obtained with an Axiovert 200 MOT microscope with Apotome correction or by confocal fluorescence microscopy on an Axiovert 200 MOT microscope with an LSM 700 confocal scanning module, and processed with the Zen 2010 software (all from Zeiss).

Measurement of mouse and human LPL levels. Mouse LPL was measured by ELISA as described previously (9). Human LPL protein was measured by a

modification of a sandwich ELISA described by Peterson *et al*. (10). Monoclonal antibody clone 5F9 was used as the trapping antibody and biotinylated monoclonal antibody 5D2 was used as the detecting antibody. Both antibodies were raised against bovine LPL. Plasma samples were denatured in 1.2 M guanidinium hydrochloride at 4° C for 1 h and diluted to 0.24 M guanidium hydrochloride before assay. Purified bovine LPL was used as a standard.

REFERENCES FOR SUPPLEMENTAL INFORMATION

1. Davies, B.S.J., Beigneux, A.P., Barnes II, R.H., Tu, Y., Gin, P., Weinstein, M.M., Nobumori, C., Nyrén, R., Goldberg, I.J., Olivecrona, G. *et al.* (2010) GPIHBP1 is responsible for the entry of lipoprotein lipase into capillaries. *Cell Metab.,* 12, 42–52.
2. Sonnenburg, W.K., Yu, D., Lee, E.C., Xiong, W., Gololobov, G., Key, B., Gay, J., Wilganowski, N., Hu, Y., Zhao, S. *et al.* (2009) GPIHBP1 stabilizes lipoprotein lipase and prevents its inhibition by angiopoietin-like 3 and angiopoietin-like 4. *J. Lipid Res.,* 50, 2421–2429.
3. Beigneux, A.P., Davies, B., Gin, P., Weinstein, M.M., Farber, E., Qiao, X., Peale, P., Bunting, S., Walzem, R.L., Wong, J.S. *et al.* (2007) Glycosylphosphatidylinositol-anchored high density lipoprotein–binding protein 1 plays a critical role in the lipolytic processing of chylomicrons. *Cell Metab.,* 5, 279–291.
4. Desai, U., Lee, E.C., Chung, K., Gao, C., Gay, J., Key, B., Hansen, G., Machajewski, D., Platt, K.A., Sands, A.T. *et al.* (2007) Lipid-lowering effects of anti-angiopoietin-like 4 antibody recapitulate the lipid phenotype found in angiopoietin-like 4 knockout mice. *Proc. Natl. Acad. Sci. U S A,* 104, 11766–11771.
5. Wang, L., Fuster, M., Sriramarao, P. and Esko, J.D. (2005) Endothelial heparan sulfate deficiency impairs L-selectin- and chemokine-mediated neutrophil trafficking during inflammatory responses. *Nature Immunol.,* 6, 902–910.
6. Levak-Frank, S., Weinstock, P.H., Hayek, T., Verdery, R., Hofmann, W., Ramakrishnan, R., Sattler, W., Breslow, J.L. and Zechner, R. (1997) Induced mutant mice expressing lipoprotein lipase exclusively in muscle have subnormal triglycerides yet reduced high density lipoprotein cholesterol levels in plasma. *J. Biol. Chem.,* 272, 17182–17190.
7. Takahashi, M., Hiyama, Y., Yokoyama, M., Yu, S., Hu, Y., Melford, K., Bensadoun, A. and Goldberg, I.J. (2008) In vivo arterial lipoprotein lipase expression augments inflammatory responses and impairs vascular dilatation. *Arterioscler. Thromb. Vasc. Biol.,* 28, 455–462.
8. Havel, R.J., Eder, H.A. and Bragdon, J.H. (1955) The distribution and chemical composition of ultracentrifugally separated lipoproteins in human serum. *J. Clin. Invest.,* 34, 1345–1353.
9. Weinstein, M.M., Yin, L., Beigneux, A.P., Davies, B.S.J., Gin, P., Estrada, K., Melford, K., Bishop, J.R., Esko, J.D., Dallinga-Thie, G.M. *et al.* (2008) Abnormal patterns of lipoprotein lipase release into the plasma in GPIHBP1-deficient mice. *J. Biol. Chem.,* 283, 34511–34518.
10. Peterson, J., Fujimoto, W.Y. and Brunzell, J.D. (1992) Human lipoprotein lipase: relationship of activity, heparin affinity, and conformation as studied with monoclonal antibodies. *J. Lipid Res.,* 33, 1165–1170.

Supplemental Movie 1

Click here to download Supplemental Movies and Spreadsheets: Movie S1.mov

Supplemental Movie 2

Click here to download Supplemental Movies and Spreadsheets: Movie S2.mov

Supplemental Movie 3

Click here to download Supplemental Movies and Spreadsheets: Movie S3.mov

Supplemental Movie 4

Click here to download Supplemental Movies and Spreadsheets: Movie S4.avi

Supplemental Movie 5

Click here to download Supplemental Movies and Spreadsheets: Movie S5.avi

Supplemental Movie 6

Click here to download Supplemental Movies and Spreadsheets: Movie S6.avi